2018

ANALYZING URBAN FLOOD DISASTERS IN EMERGING MEGACITIES USING EARTH OBSERVATIONS

Farah Nusrat
University of Rhode Island, farah_nusrat@uri.edu

ANALYZING URBAN FLOOD DISASTERS IN EMERGING MEGACITIES USING EARTH OBSERVATIONS

BY

FARAH NUSRAT

A THESIS SUBMITTED IN PARTIAL FULFILLMENT OF THE REQUIREMENTS FOR THE DEGREE OF

MASTER OF SCIENCE

IN

CIVIL AND ENVIRONMENTAL ENGINEERING

UNIVERSITY OF RHODE ISLAND

2018

MASTER OF SCIENCE

OF

FARAH NUSRAT

APPROVED:

Thesis Committee:

Major Professor Ali Shafqat Akanda

Joseph Goodwill

Soni M. Pradhanang

Nasser H. Zawia
DEAN OF THE GRADUATE SCHOOL

UNIVERSITY OF RHODE ISLAND
2018

ABSTRACT

The world is going through rapid urbanization resulting in cities turning into megacities. This rapid change turns into unplanned development in order to adapt to the growing population while the importance of the sustainability of the natural environment is neglected during the whole process. Along with the effects of climate change, flood disasters are becoming more frequent in megacities resulting in huge financial burden. Two driving factors behind urban flood disasters, anthropogenic and natural, are considered here: (i) Land Use and Land Cover (LULC) change, and (ii) intensity and frequency of precipitation. We focus on four major cities from across the world that are prone to chronic urban flooding problems: Houston, United States, Mexico City, Mexico, Jakarta, Indonesia, and Dhaka, Bangladesh. The aim of this study is to identify the main drivers behind flood disasters to improve disaster management and urban planning in these megacities. Utilizing the vantage of and recent advances in Earth Observations (EO) images and data, we assess urbanization patterns and associated hydrological changes for these cities. We found that LULC change is a principal driving factor behind urban flooding in Houston, Mexico City, and Dhaka. For Jakarta, both factors are equally important for urban flooding.

ACKNOWLEDGMENTS

First I would like to thank Allah for all the blessings that I received. Then, I would like to thank Dr. Ali Shafqat Akanda, who guided me in this tough path. Without his supervision, motivation and inspiration, I could not make this journey. I have learnt a lot of new things from him. Thank you for guiding me in exploring the research world. I want express my gratitude towards Dr. Joseph Goodwill, Dr. Soni M. Pradhanang, and Dr. Peter V. August for all the guidance and encouragement.

I would like to thank my parents, who were always there for me and gave me unconditional support and encouraged me in every possible way. Thanks to my husband, Sarfin Ony for listening to me, encouraging me and giving me mental support when I needed it most during the whole journey. I would not be me without you all. I also want to thank my friend, Sadia for giving me mental support during this journey.

Thank you all!

Farah

PREFACE

This thesis is submitted in a Manuscript Format. The first chapter is an introduction. The second chapter titled “Analyzing Urban Flood Disasters in Emerging Megacities Using Earth Observations” is prepared for submitting in Geophysical Research Letters, an American Geophysical Union (AGU) Journal.

TABLE OF CONTENTS

LIST OF TABLES

TABLE PAGE

LIST OF FIGURES

FIGURE PAGE

CHAPTER 1

Economic betterment is the root cause of the global phenomenon of rural to urban migration (Cohen, 2003). This mass movement of populations has been a vital part of the urbanization process from ancient times and continues till now (Lall, Selod, & Shalizi, 2006). Accepting the challenge of accommodating the increased population as part of the global urbanization process – cities are turning to megacities. A strong association is seen between population growth and land cover change (Dewan & Yamaguchi, 2009) while this urban expansion and growth lacks proper planning in necessary infrastructural development (Akanda & Hossain, 2012).

Urbanization is causing drastic changes in city layout and water infrastructures that are less resilient to natural disasters such as urban flooding. Land use land cover change

(K. A. Aderogba, 2012; K. Aderogba, Oredipe, Oderinde, & Afelumo, 2012; Odunuga, 2008), population growth, topography of an area, alteration in precipitation pattern and intensity, inadequate urban planning, and arbitrary solid waste disposal (Adeloye & Rustum, 2011; Lamond, Bhattacharya, & Bloch, 2012) are some of the reasons behind urban flooding. Among those, we selected two major factors, one anthropogenic and one natural, behind chronic urban flooding in emerging megacities: (i) land use land cover change – anthropogenic factor and (ii) changes of intensity and frequency of precipitation – natural factor.

The objective of this MS thesis is to uncover and understand the relative importance between (a) land use land cover change and (b) intensity and frequency change of precipitation for urban flooding. We found that LULC change is a principal driving

factor behind urban flooding in Houston, Mexico City, and Dhaka. For Jakarta, both factors are equally responsible for urban flooding.

CHAPTER 2

Analyzing Urban Flood Disasters in Emerging Megacities Using Earth Observations

By

Farah Nusrat[1], Ali Shafqat Akanda[1]

Is prepared for submission in Geophysical Research Letters, an American Geophysical Union (AGU) Journal

[1]Department of Civil and Environmental Engineering. University of Rhode Island, 1 Lippitt Rd., Bliss Hall 203. Kingston, Rhode Island 02881, United States.

Abstract

The world is going through rapid urbanization resulting in cities turning into megacities. This rapid change turns into unplanned development in order to adapt to the growing population while the importance of the sustainability of the natural environment is neglected during the whole process. Along with the effects of climate change, flood disasters are becoming more frequent in megacities resulting in huge financial burden. Two driving factors behind urban flood disasters, anthropogenic and natural, are considered here: (i) Land Use and Land Cover (LULC) change, and (ii) intensity and frequency of precipitation. We focus on four major cities from across the world that are prone to chronic urban flooding problems: Houston Metropolitan Statistical Area, United States, Mexico City, Mexico, Jakarta, Indonesia, and Dhaka, Bangladesh. The aim of this study is to identify the main drivers behind flood disasters to improve disaster management and urban planning in these megacities. Utilizing the vantage of and recent advances in Earth Observations (EO) images and data, we assess urbanization patterns and associated hydrological changes for these cities. We found that LULC change is a principal driving factor behind urban flooding in Houston, Mexico City, and Dhaka. For Jakarta, both factors are equally important for urban flooding.

Keywords: urbanization, urban flooding, Land Use and Land Cover, flood disasters, Earth Observations

1 Introduction

1.1 Background

Urban floods are an increasingly frequent and damaging environmental disasters across the globe. Due to high population growth, rapid urbanization and unplanned expansion is continuing in many regions of the planet and resulting in changes in land cover and land use (Dewan & Yamaguchi, 2009). In many developing regions of the world, this urban expansion and development lacks proper urban and regional planning and has led to large concentrations of substandard housing settlements with inadequate water, sanitation, and drainage infrastructure (Akanda & Hossain, 2012). As a result, a large portion of the world's urban dwellers has become vulnerable to natural disasters, especially during floods.

Changes in land use in many of these emerging megacities have exasperated hydrological processes and resulting flood events. Hydrological modifications from increased urbanization impact infiltration and evaporation at both temporal and spatial scales (Ali, Khan, Aslam, & Khan, 2011). Hence, runoff generation and flow patterns are altered, resulting in changes in the recurrence and severity of flooding (Ali et al., 2011). An increase in the volume of rainwater runoff and a decrease in natural storm water retention areas are also the consequences of illegal encroachment and development of catchment areas. Lack of proper solid waste management and illegal dumping of bigger populations also decrease the drainage capacity of natural canals. Land subsidence is also increasing at alarming rates in many megacities due to the unplanned extraction of groundwater (The World Bank, 2011). The gravitational capacity of natural drainage channels is hampered by land subsidence, which has

added more vulnerability to flooding and increased the risk of coastal flooding as well. The disaster risks in coastal cities are thus much greater when above factors are combined with sea-level rise and intense rainfall (The World Bank, 2011).

Change of land use is not only a physical process of transforming one land use to another but also is linked to the alteration of the social, political, economic, and cultural orientation of any society (Pangaribowo, 2018). Conversion of agricultural land to non-agricultural land is increasing to meet the land and housing requirements of growing populations, which has an impact on economy, society, and environment as well. Socio-economic factors, i.e., higher land price near the urban areas, the opportunity of diverse livelihoods, and chances of high income in urban areas, subsequently, have an impact on the land use change processes (Larasati & Hariyanto, 2018).

In this study, Houston Metropolitan Statistical Area, Texas, Mexico City, Mexico, Jakarta, Indonesia and Dhaka, Bangladesh have been chosen as example cities of urbanization and associated hydrological and land cover changes. These four major cities are all prone to chronic urban flooding problems, but each is chosen from four difference economic groups: a developed (United States), upper middle income (Mexico), and lower middle-income (Indonesia), and a recently graduated lower middle income from a least developed economy (Bangladesh). These countries have been selected to effectively compare the evolution of these trends and correlate the changes in each city's individual development contexts.

1.2 Objectives

Among many responsible driving factors, an area's topography, changes in land use and land cover (K. A. Aderogba, 2012; K. Aderogba et al., 2012; Odunuga, 2008), changes in precipitation intensity and frequency, urbanization and population growth, defective urban planning, and arbitrary solid waste disposal (Adeloye & Rustum, 2011; Lamond et al., 2012) are some important factors behind urban flooding. Among these, we investigate two major driving factors, one natural and one anthropogenic, behind the evolution of urban flooding in this study: (i) land use and land cover change, and (ii) intensity and frequency of precipitation. The goal of the study is to assess the relative importance to anthropogenic (land use land cover change) and natural (precipitation frequency and intensity) to urban flooding vulnerability and determine the strength and role of these drivers in the context of the four growing regions. The study covers the time period from 1979 to 2017, with a two-decade period (1997-2017) of overlapping availability of ground and Earth Observations (EO) of precipitation and land use land cover data.

2 Materials & Method

2.1 Study Area

In the United States, flooding is regarded as the number one among all natural disasters in terms of frequency as 28 out of 60 natural disasters were flood related between year 1980 to 2004 (Fang, Safiolea, & Bedient, 2006). Houston, Texas, ranked as the fifth largest metro area in the U.S. with a population over 7 million, is chronically vulnerable to large flooding disasters. The city is flood prone due to its close proximity to the Gulf of Mexico, the strong nature of Gulf Coast rainfall, rapid

urban growth resulting in more paved areas and roadways, the presence of clayey soils reducing infiltration, and high runoff rates along with mild slopes (Fang et al., 2006). Large flooding events in the city of Houston have occurred in 1989, 1992, 1994, 1998, 2001, 2003 (Fang et al., 2006), 2015 (Bass, Juan, Gori, Fang, & Bedient, 2016), 2016 and 2017 resulting in billions of dollars in damage and restoration costs. Over US$52 billion costs due to flood damages at counties along the Gulf of Mexico in between 2000-2005 including US$19 billion from the National Flood Insurance Program (NFIP) (Brody, Peacock, & Gunn, 2012). With current growth trends, the metro region of Houston, along with critical energy infrastructure, is likely to be highly vulnerable to future natural disasters.

Mexico City is located on the basin of Mexico, a lake basin, which is around 2260 meter above MSL. The city is surrounded by large mountains on three sides (Ochoa, Quintanar, Raga, & Baumgardner, 2015). This area had a large number of lakes and wetlands until the 1500s, and were subsequently drained and filled after the Spanish Conquest. The land cover of the city was a combination of shrubs and deciduous vegetation along with willows and pines on mountains before urbanization took place (Torres-Vera, Prol-Ledesma, & García-López, 2009). The growth of the city over the last 50 years can be divided into two groups: planned urban area for the middle and upper class population and unplanned urban areas near the periphery of the city for the poor and immigrants (Torres-Vera et al., 2009). Urbanization has intervened mostly in central and northern parts of the city whereas southern part is a blend of conserved forests, agricultural lands, wetlands and grasslands (Zambrano, Pacheco-Muñoz, & Fernández, 2018). The total urbanized area of the city consists nearly 20 million

people (Quintana-Belmares et al., 2018). A long history of illegal settlement and lack of demarcated land use between the center and the suburbs of Mexico City (Platt, 2010) led to unplanned urban development. Unceasing urban expansion along with climate change intensify spatial and temporal extent of flooding (Eakin et al., 2017). It has flooding history in the year of 1976, 1979, 1982, 1987, 1989, 1990, 1992, 1994, 1998, 1999, 2000, 2010 (Tellman et al., 2018). Most precipitation is observed between May and September with a variation in the northern and southern parts of Mexico City. The average annual precipitation in the southern areas is 1,200 mm, which is 600 mm in the northern areas (Romero Lankao, 2010).

Jakarta, the capital of Indonesia is also highly vulnerable to flooding disasters. Since 1980, Jakarta has undergone a dramatic transformation due to massive land-development projects (Padawangi & Douglass, 2015). In the last fifty years, Jakarta's population has increased from 2.7 million in 1960 to about 9 million in 2007 (Budiyono, Aerts, Brinkman, Marfai, & Ward, 2015). This drastic increase has resulted in rapid changes in land use (Verburg & Bouma, 1999). Urban areas have become denser and only one-third of the city's area remains green and unpaved (Padawangi & Douglass, 2015). Real estate developers have invested in large geographical areas to maximize profits, resulting in large-scale land development projects, shifting existing land surfaces to urban areas. Floods have become a common consequence of the significant increase in paved area. In Jakarta, devastating flooding disasters occurred in 1996, 2002, 2007 and 2013, which inundated about 40% of the city in 2007. Such massive development has also led to significant subsidence in the northern parts of the Jakarta metro area, where a number of neighborhoods often

experience coastal flooding and the old port area had to be protected by a seawall. Flood risk has dramatically increased due to population growth and a subsidence rate of 10 cm/year in some areas (Brinkman & Hartman, 2008).

Dhaka, the capital city of Bangladesh is an example of unplanned urbanization. It is one of the most densely populated cities in the world, with the highest growth rate in unplanned settlements (Akanda & Hossain, 2012). The population of Dhaka has increased from 3.44 million in 1981 (Dewan & Yamaguchi, 2009) to about 18 million in 2017 (The World Bank, 2017). Most of this growth have been absolved in unplanned settlements, where a large number of people have moved in from rural areas as economic migrants, climate refugees, and victims of natural disasters. Dhaka has an annual mean rainfall of 1920 mm and heaviest rainfalls occur between June and August (Hossain, Fien, & Horne, 2018). The city was originally developed in flood-free high lands, but the recent occupation of low-lying riparian suburbs around the city has drastically increased the flood vulnerability of the people (Adikari, Osti, & Noro, 2010). Low lying lands, rivers, canal, and water bodies are increasingly being filled to construct new accommodations on lands that previously worked as natural drainage channels (Hassan & Southworth, 2017). Artificial drainage is also hampered due to poor design of drains and sewer networks, unplanned construction, and dumping of uncollected wastes on the roadside (Yasmin & Rahman, 2017). Wetlands also operate as a recharge source of groundwater storage and allow drainage of extra precipitation that may otherwise cause urban flooding (IRIN, 2012). Thus, their recession has made the city more vulnerable to larger flooding events (IRIN, 2012). In addition, there is an embankment surrounding the Dhaka city to protect from river flooding. During

monsoon, river water levels are often higher than the city's water level inside the embankment, which creates hindrance in drainage by gravity (Mark, Wennberg, Van Kalken, Rabbi, & Albinsson, 1998).

2.2 Data

2.2.1 Landsat Images

All Landsat images for Houston, Jakarta and Dhaka were collected from the United States Geological Survey (USGS) Earth Explorer (USGS, 2017). Three years with decadal frequency were selected for comparison: 1997, 2007, and 2017. All images have a spatial resolution of 30 m. Only day-time images with cloud cover less than 10% were used for this analysis to allow the best visibility of land use and land cover. Landsat 5 imagery was used for 1997 and 2007, while Landsat 8 (launched in 2013) imagery was used for 2017.

2.2.2 Precipitation Data

We collected precipitation data (TRMM_3B42_Daily) from Tropical Rainfall Measuring Mission (TRMM) using the GES-DISC (Goddard Earth Sciences Data and Information Services Center) (Goddard Earth Sciences Data and Information Services Center (GES DISC), n.d.) for the specific Area of Interest (AOI) for the year of 1998 to 2017. The spatial resolution is 0.25° x 0.25° and temporal resolution is 1 day. The precipitation time-series is aggregated to several temporal scales (weekly, monthly, seasonal, and annual) for anomalies and trend analyses. Mann Kendall trend analysis and Sens's Slope is determined to better understand the statistically significant change in the precipitation trend. Trend of monthly maximum rainfall, total monthly rainfall, number of rainy days per month, total annual rainfall, maximum Consecutive Wet

Days (CWD) in a year (annually maximum number of consecutive days with precipitation ≥ 1 mm), R10 (number of days annually when precipitation ≥ 10 mm), R20 (number of days annually when precipitation ≥ 20 mm), monthly and seasonal rainfall for each area were calculated. For longer-term trend analysis, CPC Global Unified Gauge-Based Analysis of Daily Precipitation (1979-2017) data (NOAA/OAR/ESRL PSD, Boulder, Colorado, n.d.) were collected for Houston and Jakarta. Bangladesh Meteorological Department Data (1953-2017) were collected for Dhaka. In CPC Global Unified Gauge-Based Analysis of Daily Precipitation, long range precipitation data are not available for Mexico. So TRMM data were used for trend analysis and SPI calculation of Mexico City.

2.3 Method

(a) Detecting changes in LULC using Landsat Images:

For Landsat 5 images, bands 1 to 5 were stacked to a single layer; and for Landsat 8 images, another layer was created by stacking bands 2 to 6. As we compared images in this study, we stacked bands of Landsat images with similar wavelengths (μm). A subset was created with each stacked layer according to the Area of Interest (AOI) and then unsupervised image classification with 40 classes is done. With the help of ERDAS IMAGINE 2016 software, each class was geo-referenced with Google Earth image of that particular period and assigned to a specific land cover: urban areas, vegetative cover, waterbodies, barren land, sand filled areas, future housing projects, and forest land. This helps to visualize the changes in land use/land cover over time. In the post classification process, urban areas were used as masks to detect other land

uses that were transformed to urban land use and the area calculation was done in acres.

(b) Creating land use/land cover change index:

The land use/land cover change index was created on the basis of infiltration capacity in this study. The lands which have more infiltration or drainage capability and transferred to paved areas are categorized with the highest index. The determination of the land-use index is shown in Table 1.

Table 1: Land use/land cover change index on the basis of infiltration capacity

Initial Land use	**Transformed Land use**	**Land Use/Land Cover Change Index**
Waterbodies	Urban Area	7
Vegetative Cover	Urban Area	6
Forest Land	Urban Area	5
Barren Land	Urban Area	4
Future Housing Projects	Urban Area	3
Sand filled Area (compacted)	Urban Area	2
Urban Area	Urban Area (No change)	1

(c) Non-parametric Mann-Kendall (MK) Trend Test

To determine the monotonic increasing or decreasing trend of climatological variables, non-parametric Mann-Kendall (MK) test (Mann, 1945) & (Kendall, 1955) ((Yu, Zou,

& Whittemore, 1993); (Douglas, Vogel, & Kroll, 2000); (Singh, Kumar, Thomas, & Arora, 2008)) is highly used due to its accommodating ability of missing values (Gajbhiye, Meshram, Mirabbasi, & Sharma, 2016). In this trend test, the null hypothesis (H_0) is there is no monotonic trend in the precipitation over time and the alternative hypothesis (H_A) is there is a monotonic trend (increasing or decreasing) available in precipitation over time. In any rainfall trend analysis, outliers will be there due to extreme rainfall events. These outliers have less impact (Birsan, Molnar, Burlando, & Pfaundler, 2005) on the result of this MK test as its statistics is based on positive or negative sign rather than any value (Gajbhiye et al., 2016). Here, "modifiedmk" package of RStudio software is used to determine the Mann-Kendal Trend and Sen's slope. We assume that the rainfall time series is independent.

$$S = \sum_{i=1}^{n-1} \sum_{j=i+1}^{n} sign(x_j - x_i) \quad (1)$$

where x_i and x_j are sequential data for the *i*th and *j*th terms, sign is the signum function, and *n* is the sample size.

$$sign(x_i - x_j) = \begin{cases} +1, & if\ x_j - x_i > 1 \\ 0, & if\ x_j - x_i = 0 \\ -1, & if\ x_j - x_i < 1 \end{cases} \quad (2)$$

The statistic *S* is nearly Gaussian when $n = 18$ with the mean $E(S)$ and variance $\mathrm{Var}(S)$ of the statistic *S* given by

$$E(S) = 0, Var\ (S) = \frac{n(n+1)(2n+5)}{18} \quad (3)$$

If there is tie in the dataset, then Var (S) has to be adjusted and becomes

$$Var(S) = \frac{1}{18}\{n(n-1)(2n+5) - \sum_{p=1}^{q} t_p\ (t_p - 1)(2t_p + 5)\} \quad (4)$$

The variable q and t_p are the number of tied groups and number of data values in the *p*th group, respectively. The standardized statistic (*Z*) for one-tailed test of the statistic *S* is given as follows:

$$Z_{mk} = \begin{cases} \frac{S-1}{\sqrt{Var(S)}} & if\ S > 0 \\ 0 & if\ S = 0 \\ \frac{S+1}{\sqrt{Var(S)}} & if\ S < 0 \end{cases} \quad (5)$$

An increasing trend is identified with a positive Z_{mk} and a decreasing trend is identified with a negative Z_{mk}. For 95% confidence interval (or significance level, α= 0.05, the critical Z value = $\pm$ 1.96 (for a two tailed test) and for 90% confidence interval, |*Z*| = 1.65 (Q. Zhang, Xu, & Zhang, 2009). If |*Z*| > 1.96 (Q. Zhang et al., 2009), the null hypothesis can be rejected. For 99% confidence interval, |Z| = 2.58 (Q. Zhang et al., 2009).

Sen's Slope

The magnitude of the trend change can be identified by a slope estimator β, which was first proposed by Sen (Sen, 1968) and then extended by Hirsch (Hirsch, Slack, & Smith, 1982). β is the median of overall all possible combinations of pairs for the whole dataset. The magnitude of trend was calculated predicted by the Sen's slope estimator with the slope T_i of all data pairs was computed as follows:

$$T_i = \frac{x_j - x_i}{j - i} \quad (6)$$

Where x_j and x_i are considered as data values at time *j* and *I* (*j* > *i*) correspondingly. The median of these *N* values of T_i is represented as Sen's estimator of slope. Sen's estimator is computed as

$$Q_{med} = \frac{T(N+1)}{2} \quad (7)$$

when N is odd, and it is considered as

$$Q_{med} = \frac{\left[T\left(\frac{N}{2}\right)+\frac{T(N+2)}{2}\right]}{2} \quad (8)$$

when N is even. At the end, Q_{med} is computed by two-sided test at $100\,(1-\alpha)\,\%$ confidence interval, and then a true slope can be obtained by the non-parametric test. A positive value of Q_i indicates an upward or increasing trend, and a negative value gives a downward or decreasing trend in the time series.

(d) Standardized Precipitation Index (SPI):

Standardized Precipitation Index (SPI) was calculated for determining flood risks. SPI is generally used for monitoring drought (McKee, 1995) (McKee, Doesken, & Kleist, 1993) but has also been used to identify flood conditions where SPI can detect the development of soil-saturation conditions (Seiler, Hayes, & Bressan, 2002). SPI can be calculated for various temporal scales such as 1 month, 3 months, 6 months, 12 months, 24 months. SPI for 1 month is used here as the most relevant measure for appropriate soil moisture conditions for flooding. Long term precipitation data are required to calculate SPI, then the probability distribution function (Hayes, Svoboda, Wilhite, & Vanyarkho, 1999) is obtained from the data. Then, the cumulative distribution is transferred to normal distribution with a standard deviation of one, keeping zero as a mean value. Any positive SPI value indicates greater than median precipitation and vice versa. In 2000, Hayes et al. reported the interpretation of the Standardized Precipitation Index values (Hayes, 2000) into soil wetness measurements. The theoretical probability (Bonaccorso, Cancelliere, & Rossi, 2015) of occurrence of each interpretation derived from normal probability density function (Guhathakurta, Menon, Inkane, Krishnan, & Sable, 2018) is also given below:

Table 2: Standardized Precipitation Index (SPI) ranges

SPI	Interpretation	Theoretical Probability
2.0 +	Extremely Wet	2.3
1.5 to 1.99	Very Wet	4.4
1.0 to 1.49	Moderately Wet	9.2
-0.99 to 0.99	Near Normal	68.2
-1.0 to -1.49	Moderately Dry	9.2
-1.5 to -1.99	Severely Dry	4.4
-2.0 and less	Extremely Dry	2.3

(e) Risk Index:

Using the land use/land cover change index and the SPI, the risk index was created and transferred to a flood risk map for four cities for different months. Each SPI range has a probability of occurrence. Multiplying the SPI with LULC change index is giving us a probability which can be termed as risk index, which will give us an idea about how much urban flood risk any area has in terms of LULC change and precipitation alteration. The equation of risk index and the interpretation of the risk index range is given below.

Risk Index = Land Use/Land Cover Change Index X SPI (9)

Table 3: Risk Index and interpretation

Risk Index Range	Interpretation
≤0	No Risk
0.01-6.00	Low Risk
6.01-12.00	Moderate Risk
12.01-18.00	High Risk
18.01-21.00	Extreme Risk

The flowchart of the methodology of this study is outlined below in Figure 1.

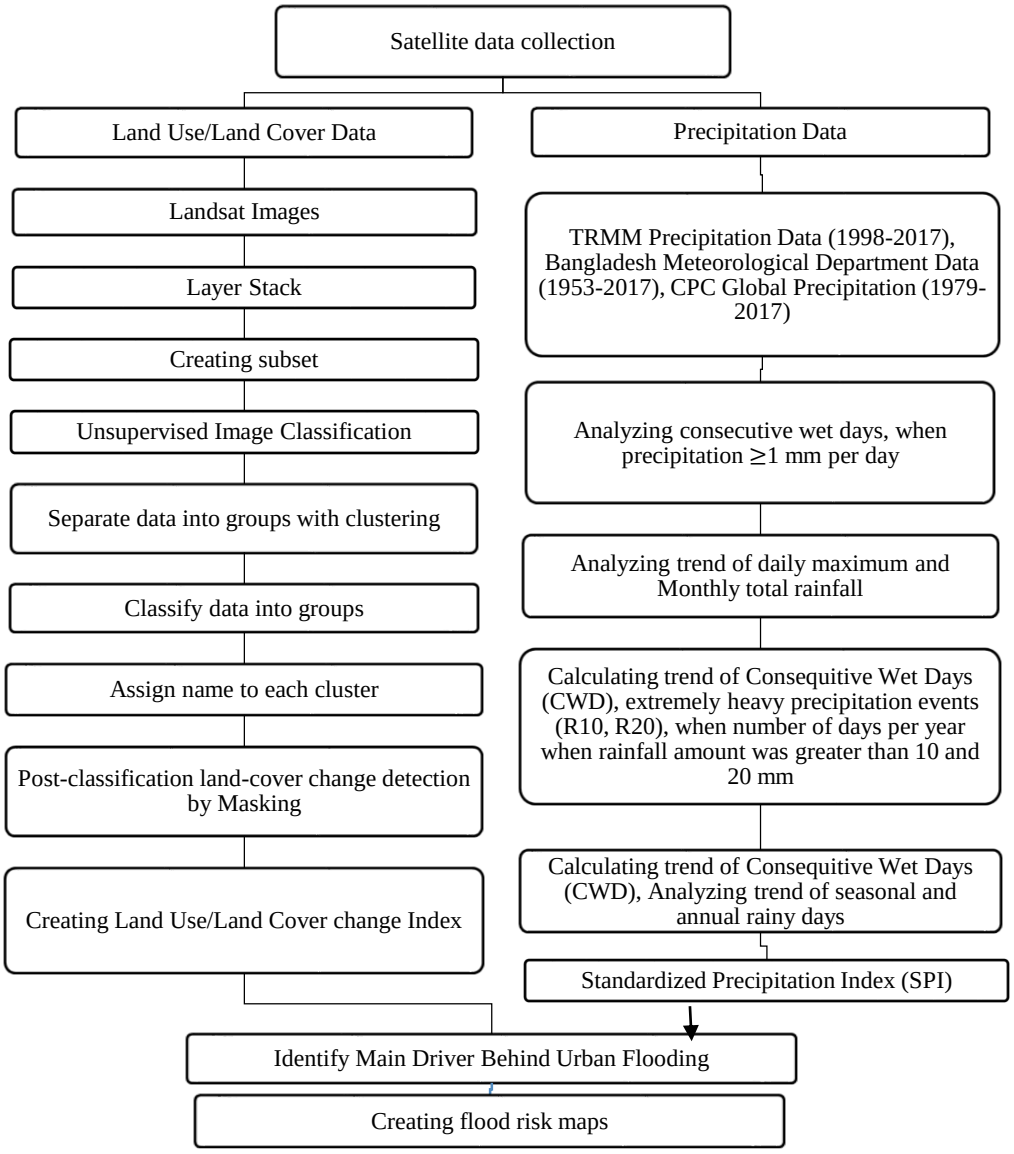

Figure 1: Land Use Land Cover Change Index using Landsat imagery (left column) and precipitation index using TRMM, CPC & BMD data (right column) were independently processed then findings are merged to identify the Urban Flood Risk.

3 Results

Land Use and Land Cover Data Analysis

In Houston, forest land and urban areas are the most changed land use and land cover categories from 1997 to 2017 (figure 2A-2C). According to figure 2A-2C, 33% of the total area was forest land in 1997 which was reduced to 20% in 2017. Vegetative cover was 29% of the total area in 1997 and has decreased to 24% in 2017. The percentage of barren land in 1997 was 3% of the total area, which has increased to 8% in 2017. Urban area, the most dominating land use in Houston, has increased from 31% to 45% between 1997 and 2017. Between 1997 to 2007, around 141,680 acres of different land covers were converted to urban areas, the changed land cover amount is 120,390 acres between 2007 and 2017.

In Mexico City, increase of barren land is observed from 1997 to 2007, which shows a decrease in 2017 (Figure 2D-2F). Urban area has increased from 33% to 37% of the total area from 1997 to 2017. Vegetative cover, which was 25% in 1997, is decreased to 22% in 2017. Around 35,000 acres and 54,000 acres of different land covers were converted to urban area in 1997 to 2007 and 2007 to 2017 respectively.

Table 4: Land use/ Land cover changes from 1997 to 2017 in Houston, and Mexico City

Land Cover/ Land use	Houston Metropolitan Statistical Area (acres)			Mexico City (acres)		
	year 1997	year 2007	year 2017	year 1997	year 2007	year 2017
Barren Land	29,475	53,843	71,783	51,235	60,159	44,274
Forest Land	299,820	267,997	181,988	201,980	177,932	195,658

Land Cover/ Land use	Houston Metropolitan Statistical Area (acres)			Mexico City (acres)		
	year 1997	year 2007	year 2017	year 1997	year 2007	year 2017
Urban Area	282,092	348,966	405,239	206,679	208,183	232,631
Vegetative Cover	262,610	201,341	214,019	158,016	168,633	139,357
Water	10,584	15,286	19,252	3,814	6,816	9,804
Sand Filling	15,253	12,402	7,555			
Future Housing Projects						
Total Area	899,835	899,835	899,835	621,724	621,724	621,724

Extreme growth of urbanization is observed in Jakarta between the year 1997 to 2017. During this 20 years, urban areas have increased from 41% to 60% of the total area, which clearly reflects the haphazard urban expansion pattern. Apart from urban areas, vegetative cover and barren land are the two most changed land covers in this 20 years of span, both showing decreasing trends (Figure 2G-2I). 3% of the total area was designated as future housing projects in 2007 which is altered to urban areas in 2017. Around 48,000 acres of different land covers were transferred to urban areas between 1997 to 2007, which is increased to 69,000 acres between 2007 to 2017.

In Dhaka, vegetative cover and urban area are the two most changed land use and land covers among all the land use and land covers categories. From 2007, two new land uses and land covers are observed in Dhaka: sand filled areas and future housing projects, where both show increasing trends between 2007 and 2017. In 1997, vegetative cover consists 60% of the total area, which is reduced to 34% in 2017 (Figure 2J-2L). The percentage of urban area in 2017 has increased 1.5 times from that observed in 1997. The area that changed from different land covers to urban areas were 38,000 acres and 40,500 acres in 1997 to 2007 and 2007 to 2017 respectively. In 2017, 11% area of Dhaka city is designated as new housing projects apart from the existing urban area. These urban housing projects are not finished yet and will add more paved area in the city after completion.

Table 5: Land use/ Land cover changes from 1997 to 2017 in Jakarta, and Dhaka

Land Cover/ Land use	Jakarta (acres)			Dhaka (acres)		
	year 1997	year 2007	year 2017	year 1997	year 2007	year 2017
Barren Land	39,544	18,134	3,586	7,442	11,908	12,239
Forest Land	70,678	54,810	73,810	47,441	64,225	55,191
Urban Area	145,052	159,137	210,043	52,845	65,959	80,532
Vegetative Cover	64,588	81,860	35,691	189,984	147,469	106,299
Water	29,857	26,800	26,590	17,220	16,282	17,792
Sand Filling					3,565	7,524
Future Housing		8,977			5,524.51	35,355.24

Land Cover/ Land use	Jakarta (acres)			Dhaka (acres)		
	year 1997	year 2007	year 2017	year 1997	year 2007	year 2017
Projects						
Total Area	349,719	349,719	349,719	314,933	314,933	314,933

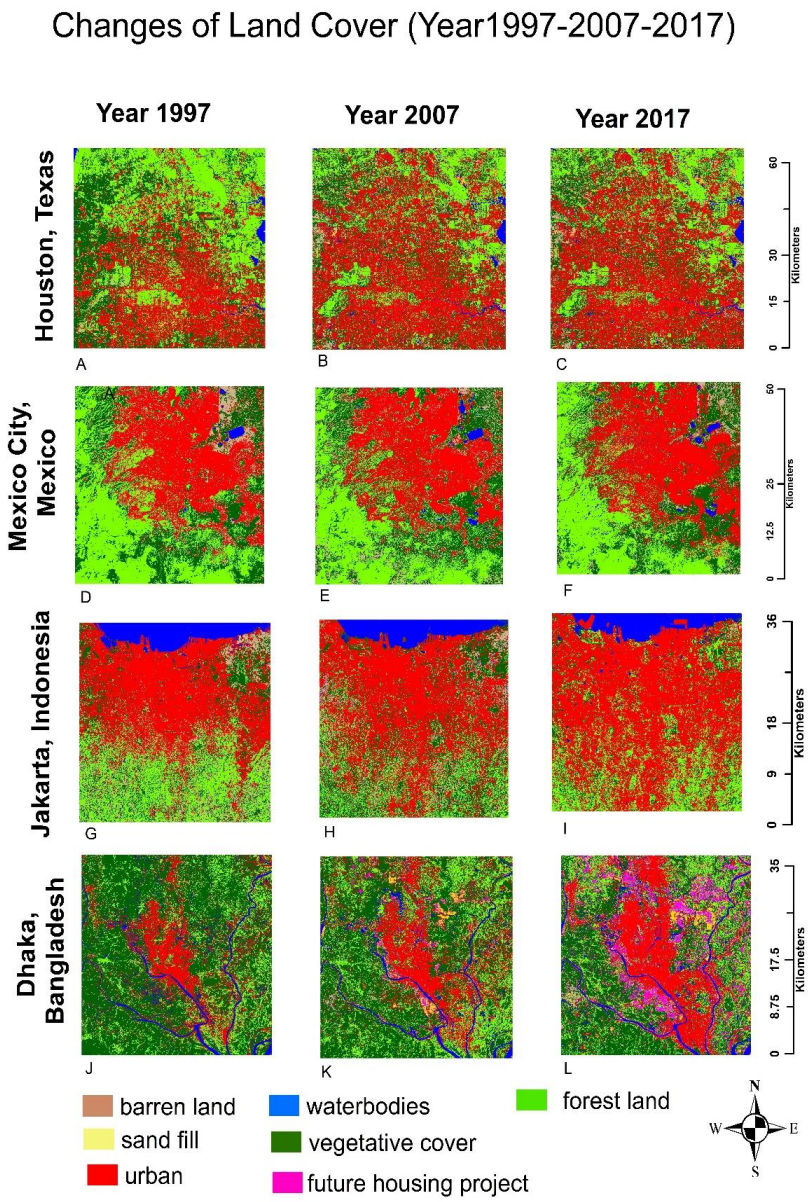

Figure 2: Decadal Land use / Land cover changes from 1997 to 2017 in Houston (2A, 2B, 2C), Mexico City (2D, 2E, 2F), Jakarta (2G, 2H, 2I) and Dhaka (2J, 2K, 2L). The expansion of urban growth and transformation of other land uses and land covers to urban area in these cities with respect to times are shown in this figure.

Precipitation Analysis

(i) Detection of Mann-Kendall Trend Test and Sen's Slope

Mann-Kendall trend test was accomplished on the TRMM data, Bangladesh Meteorological Department (BMD) data, and Climate Prediction Center (CPC) Global Unified Gauge-Based Analysis of Daily Precipitation dataset for each of the study area. The test determines the trend change of monthly maximum rainfall, total monthly rainfall, number of rainy days per month, total annual rainfall, maximum Consecutive Wet Days (CWD) in a year (annually maximum number of consecutive days with precipitation ≥ 1 mm), R10 (number of days annually when precipitation ≥ 10 mm), R20 (number of days annually when precipitation ≥ 20 mm), monthly and seasonal rainfall for each area. For 95% confidence interval (or significance level, α= 0.05, the critical Z value = $\pm$ 1.96 (for a two tailed test) and for 90% confidence interval, $|Z| = 1.65$ (Q. Zhang et al., 2009). If $|Z| > 1.96$ (Q. Zhang et al., 2009), the null hypothesis can be rejected. For 99% confidence interval, $|Z| = 2.58$ (Q. Zhang et al., 2009).

In both locations of Houston (using CPC data), the monthly total precipitation in January, March, May, July, September, October, November and August (in location 2 only) is showing negative trend as both Z and Sen's slope is negative for these months but not statistically significant except the month of July for location 2. Same months showed negative trend in daily maximum rainfall analysis also, where July is showing statistically significant decreasing trend in both locations. In both locations, the trends of annual rainfall, R10, R20, total and maximum rainfall of summer, winter, spring, fall, dry and wet season are decreasing. Consecutive Wet Days (CWD) showed an

increasing trend in both locations, which are not statistically significant. For Mexico, maximum and total rainfall in dry months are showing positive trend and it shows decreasing trend for wet months. R10 and R20 is showing increasing trend, whereas CWD and annual rainfall in showing decreasing trend. None of them is statistically significant. The wet months of Mexico City is from May to October. Negative Z value and Sen's slope is observed in monthly total rainfall, daily maximum rainfall and number of wet days in those wet season months, which matches with the decreasing trend of annual rainfall and CWD. A long data series can help to better understand the trend. In Jakarta, the total and maximum rainfall in wet and dry period is showing positive trend along with positive Sen's slope. As one of the wet period months, January is only showing decreasing trend in monthly total, daily maximum and number of wet days on that month. February is showing statistically significant positive trend in monthly total and daily maximum. The trend of total and maximum rainfall for January-March is showing statistically significant positive trend. For Dhaka, the daily maximum rainfall trend for monsoon months (Jun-August) along with one pre-monsoon month (May) showing decreasing trend. Number of rainy days in monsoon months (June, August) showing decrease, which is statistically significant for June only. Maximum and total rainfall trend in monsoon and wet periods, annual rainfall and CWD are decreasing and only R10 and R20 is showing positive trend for Dhaka. The result of the Mann Kendal Trend Analysis and Sen's Slope are given below:

Table 6: Mann Kendal Trend Analysis and Sen's Slope Analysis of Houston, CPC Location 1

Trend detection of station data of Houston, CPC Location 1 (1979-2017)							
Mann-Kendall Trend Test & Sen's Slope							
Indicators		Z-Value	Sen's slope	S	Var(S)	p value	Tau
Monthly Total Rainfall	January	-1.016	-0.922	-85	6833.667	0.310	-0.115
	February	0.363	0.288	31	6833.667	0.717	0.042
	March	-0.823	-0.991	-69	6833.667	0.411	-0.093
	April	0.169	0.132	15	6833.667	0.866	0.020
	May	-0.871	-0.556	-73	6833.667	0.384	-0.099
	June	0.774	0.903	65	6833.667	0.439	0.088
	July	-1.669*	-2.404	-139	6833.667	0.095	-0.188
	August	0.024	0.029	3	6833.667	0.981	0.004
	September	-0.387	-0.590	-33	6833.667	0.699	-0.045
	October	-0.629	-0.583	-53	6833.667	0.529	-0.072
	November	-0.556	-0.573	-47	6833.667	0.578	-0.063
	December	0.653	0.470	55	6833.667	0.514	0.074

Trend detection of station data of Houston, CPC Location 1 (1979-2017)							
Mann-Kendall Trend Test & Sen's Slope							
Indicators		Z-Value	Sen's slope	S	Var(S)	p value	Tau
Daily Maximum Rainfall	January	-0.073	-0.021	-7	6833.667	0.942	-0.009
	February	0.508	0.208	43	6833.667	0.611	0.058
	March	-0.097	-0.030	-9	6833.667	0.923	-0.012
	April	0.653	0.217	55	6833.667	0.514	0.074
	May	-0.944	-0.221	-79	6833.667	0.345	-0.107
	June	0.895	0.337	75	6833.667	0.371	0.101
	July	-1.984*	-0.723	-165	6833.667	0.047	-0.223
	August	-1.258	-0.477	-105	6833.667	0.208	-0.142
	September	-0.532	-0.213	-45	6833.667	0.595	-0.061
	October	-0.460	-0.190	-39	6833.667	0.646	-0.053
	November	-0.435	-0.179	-37	6833.667	0.663	-0.050
	December	0.508	0.143	43	6833.667	0.611	0.058

Trend detection of station data of Houston, CPC Location 1 (1979-2017)							
Mann-Kendall Trend Test & Sen's Slope							
Indicators		Z-Value	Sen's slope	S	Var(S)	p value	Tau
No. of Rainy days (Rainfall >= 1mm)	January	-2.327**	-0.118	-192	6739.333	0.020	-0.259
	February	-0.292	0.000	-25	6740.333	0.770	-0.034
	March	-1.458	-0.083	-121	6775.667	0.145	-0.163
	April	-1.923*	-0.087	-158	6664.667	0.054	-0.213
	May	-1.253	-0.061	-104	6758.000	0.210	-0.140
	June	0.304	0.000	26	6774.667	0.761	0.035
	July	-0.474	0.000	-40	6758.667	0.635	-0.054
	August	0.293	0.000	25	6732.333	0.770	0.034
	September	0.328	0.000	28	6762.000	0.743	0.038
	October	-0.859	0.000	-71	6645.667	0.391	-0.096
	November	-1.720*	-0.071	-142	6718.000	0.085	-0.192
	December	-0.134	0.000	-12	6722.667	0.893	-0.016
Annual Rainfall		-1.476	-6.175	-123	6833.667	0.140	-0.166

Trend detection of station data of Houston, CPC Location 1 (1979-2017)						
Mann-Kendall Trend Test & Sen's Slope						
Indicators	Z-Value	Sen's slope	S	Var(S)	p value	Tau
Consecutive Wet Days (CWD)	0.110	0.000	10	6676.667	0.912	0.013
R10	-1.079	-0.138	-90	6809.333	0.281	-0.121
R20	-1.894*	-0.162	-157	6786.333	0.058	-0.212
Total Rainfall of Spring	-1.331	-2.707	-111	6833.667	0.183	-0.150
Total Rainfall of Summer	-0.508	-1.536	-43	6833.667	0.611	-0.058
Total Rainfall of Fall	-1.427	-2.437	-119	6833.667	0.153	-0.161
Total Rainfall of Winter	-0.266	-0.299	-23	6833.667	0.790	-0.031
Maximum Rainfall in Spring	-1.282	-1.317	-107	6833.667	0.200	-0.144

Trend detection of station data of Houston, CPC Location 1 (1979-2017)						
Mann-Kendall Trend Test & Sen's Slope						
Indicators	Z-Value	Sen's slope	S	Var(S)	p value	Tau
Maximum Rainfall in Summer	-1.282	-2.005	-107	6833.667	0.200	-0.144
Maximum Rainfall in Fall	-0.677	-0.694	-57	6833.667	0.498	-0.077
Maximum Rainfall in Winter	-1.065	-0.781	-89	6833.667	0.287	-0.120
Total Rainfall in Wet Season (MAR-NOV)	-1.766*	-6.282	-147	6833.667	0.077	-0.198
Total Rainfall in Dry Season (DEC-FEB)	-0.266	-0.299	-23	6833.667	0.790	-0.031
Maximum Rainfall in Wet Season (MAR-NOV)	-1.355	-1.888	-113	6833.667	0.175	-0.152

Trend detection of station data of Houston, CPC Location 1 (1979-2017)						
Mann-Kendall Trend Test & Sen's Slope						
Indicators	Z-Value	Sen's slope	S	Var(S)	p value	Tau
Maximum Rainfall in Dry Season (DEC-FEB)	-1.065	-0.781	-89	6833.667	0.287	-0.120

95% confidence interval (**), 90% confidence interval (*)

Table 7: Mann Kendal Trend Analysis and Sen's Slope Analysis of Houston, CPC Location 2

Trend detection of station data of Houston, CPC Location 2 (1979-2017)							
Mann-Kendall Trend Test & Sen's Slope							
Indicators		Z-Value	Sen's slope	S	Var(S)	P-value	Tau
Monthly Total Rainfall	January	-0.847	-0.833	-71	6833.667	0.397	-0.096
	February	-0.097	-0.122	-9	6833.667	0.923	-0.012
	March	-1.065	-1.087	-89	6833.667	0.287	-0.120
	April	0.290	0.340	25	6833.667	0.772	0.034

Trend detection of station data of Houston, CPC Location 2 (1979-2017)							
Mann-Kendall Trend Test & Sen's Slope							
Indicators		Z-Value	Sen's slope	S	Var(S)	P-value	Tau
	May	-0.774	-0.322	-65	6833.667	0.439	-0.088
	June	0.750	0.537	63	6833.667	0.453	0.085
	July	-2.226**	-2.472	-185	6833.667	0.026	-0.250
	August	-0.387	-0.378	-33	6833.667	0.699	-0.045
	September	-1.016	-0.978	-85	6833.667	0.310	-0.115
	October	-1.137	-0.938	-95	6833.667	0.255	-0.128
	November	-0.798	-0.604	-67	6833.667	0.425	-0.090
	December	0.992	0.713	83	6833.667	0.321	0.112
Daily Maximum Rainfall	January	0.000	-0.004	-1	6833.667	1.000	-0.001
	February	0.460	0.117	39	6833.667	0.646	0.053
	March	-0.290	-0.152	-25	6833.667	0.772	-0.034
	April	0.944	0.255	79	6833.667	0.345	0.107
	May	-0.992	-0.193	-83	6833.667	0.321	-0.112

Trend detection of station data of Houston, CPC Location 2 (1979-2017)							
Mann-Kendall Trend Test & Sen's Slope							
Indicators		Z-Value	Sen's slope	S	Var(S)	P-value	Tau
	June	0.968	0.313	81	6833.667	0.333	0.109
	July	-2.153**	-0.629	-179	6833.667	0.031	-0.242
	August	-1.718*	-0.393	-143	6833.667	0.086	-0.193
	September	-0.290	-0.105	-25	6833.667	0.772	-0.034
	October	-0.823	-0.356	-69	6833.667	0.411	-0.093
	November	-0.653	-0.221	-55	6833.667	0.514	-0.074
	December	0.895	0.252	75	6833.667	0.371	0.101
No. of Rainy days (Rainfall >= 1mm)	January	-1.962**	-0.097	-162	6735.333	0.050	-0.219
	February	-1.134	-0.056	-94	6726.667	0.257	-0.127
	March	-1.630	-0.094	-135	6757.000	0.103	-0.182
	April	-1.976**	-0.083	-163	6724.333	0.048	-0.220
	May	-0.815	-0.037	-68	6753.333	0.415	-0.092
	June	1.033	0.069	86	6765.333	0.301	0.116

Trend detection of station data of Houston, CPC Location 2 (1979-2017)							
Mann-Kendall Trend Test & Sen's Slope							
Indicators		Z-Value	Sen's slope	S	Var(S)	P-value	Tau
	July	-0.243	0.000	-21	6751.000	0.808	-0.028
	August	0.000	0.000	1	6745.000	1.000	0.001
	September	-1.044	-0.069	-87	6781.667	0.296	-0.117
	October	-0.904	-0.032	-75	6703.000	0.366	-0.101
	November	-1.822*	-0.077	-150	6690.667	0.069	-0.202
	December	-0.757	0.000	-63	6708.333	0.449	-0.085
Annual Rainfall		-2.008**	-6.995	-167	6833.667	0.045	-0.225
Consecutive Wet Days (CWD)		0.061	0.000	6	6737.333	0.951	0.008
R10		-1.541	-0.185	-128	6791.333	0.123	-0.173
R20		-1.639	-0.143	-136	6780.667	0.101	-0.184
Total Rainfall of Spring		-1.331	-2.427	-111	6833.667	0.183	-0.150

Trend detection of station data of Houston, CPC Location 2 (1979-2017)						
Mann-Kendall Trend Test & Sen's Slope						
Indicators	Z-Value	Sen's slope	S	Var(S)	P-value	Tau
Total Rainfall of Summer	-0.847	-1.684	-71	6833.667	0.397	-0.096
Total Rainfall of Fall	-1.790*	-3.125	-149	6833.667	0.073	-0.201
Total Rainfall of Winter	-0.290	-0.242	-25	6833.667	0.772	-0.034
Maximum Rainfall in Spring	-1.185	-1.092	-99	6833.667	0.236	-0.134
Maximum Rainfall in Summer	-2.056**	-2.621	-171	6833.667	0.040	-0.231
Maximum Rainfall in Fall	-1.258	-1.228	-105	6833.667	0.208	-0.142
Maximum Rainfall in Winter	-0.750	-0.459	-63	6833.667	0.453	-0.085

Trend detection of station data of Houston, CPC Location 2 (1979-2017)						
Mann-Kendall Trend Test & Sen's Slope						
Indicators	Z-Value	Sen's slope	S	Var(S)	P-value	Tau
Total Rainfall in Wet Season (MAR-NOV)	-2.032**	-6.693	-169	6833.667	0.042	-0.228
Total Rainfall in Dry Season (DEC-FEB)	-0.290	-0.242	-25	6833.667	0.772	-0.034
Maximum Rainfall in Wet Season (MAR-NOV)	-1.935*	-2.480	-161	6833.667	0.053	-0.217
Maximum Rainfall in Dry Season (DEC-FEB)	-0.750	-0.459	-63	6833.667	0.453	-0.085

95% confidence interval (**), 90% confidence interval (*)

Table 8: Mann Kendal Trend Analysis and Sen's Slope Analysis of Mexico City, TRMM Location 5

Trend detection of Mexico City, TRMM (1998-2017)							
Mann-Kendall Test & Sen's Slope							
Indicators		Z-Value	Sen's slope	S	Var(S)	P-value	Tau
Monthly Total Rainfall	January	0.357	0.077	12	950.000	0.721	0.063
	February	-0.519	-0.087	-17	949.000	0.603	-0.089
	March	1.006	0.666	32	950.000	0.315	0.168
	April	0.292	0.243	10	950.000	0.770	0.053
	May	1.460	2.633	46	950.000	0.144	0.242
	June	-0.422	-0.773	-14	950.000	0.673	-0.074
	July	0.941	0.959	30	950.000	0.347	0.158
	August	-0.357	-0.366	-12	950.000	0.721	-0.063
	September	-0.876	-2.520	-28	950.000	0.381	-0.147
	October	-1.914*	-2.354	-60	950.000	0.056	-0.316
	November	-0.032	-0.015	-2	950.000	0.974	-0.011

Trend detection of Mexico City, TRMM (1998-2017)							
Mann-Kendall Test & Sen's Slope							
Indicators		Z-Value	Sen's slope	S	Var(S)	P-value	Tau
	December	-1.720(	-0.210	-54	950.000	0.086	-0.284
Daily Maximum Rainfall	January	0.097	0.017	4	950.000	0.922	0.021
	February	-0.519	-0.054	-17	949.000	0.603	-0.089
	March	1.395	0.300	44	950.000	0.163	0.232
	April	1.655*	0.411	52	950.000	0.098	0.274
	May	1.330	0.729	42	950.000	0.183	0.221
	June	-0.357	-0.102	-12	950.000	0.721	-0.063
	July	-0.162	-0.051	-6	950.000	0.871	-0.032
	August	1.006	0.802	32	950.000	0.315	0.168
	September	-1.460	-0.449	-46	950.000	0.144	-0.242
	October	-0.357	-0.140	-12	950.000	0.721	-0.063
	November	0.876	0.128	28	950.000	0.381	0.147
	December	-0.487	-0.019	-16	950.000	0.626	-0.084

Trend detection of Mexico City, TRMM (1998-2017)							
Mann-Kendall Test & Sen's Slope							
Indicators		Z-Value	Sen's slope	S	Var(S)	P-value	Tau
No. of Rainy days (Rainfall >= 1mm)	January	0.132	0.000	5	915.000	0.895	0.026
	February	-1.100	-0.056	-34	899.333	0.271	-0.179
	March	0.624	0.068	20	926.000	0.532	0.105
	April	-1.310	-0.154	-41	933.000	0.190	-0.216
	May	1.113	0.222	35	933.000	0.266	0.184
	June	-0.491	-0.059	-16	932.667	0.623	-0.084
	July	-0.426	0.000	-14	930.667	0.670	-0.074
	August	-2.819***	-0.317	-87	931.000	0.005	-0.458
	September	-0.982	-0.191	-31	933.667	0.326	-0.163
	October	-2.280**	-0.500	-71	942.333	0.023	-0.374
	November	-0.230	0.000	-8	930.000	0.818	-0.042
	December	-0.036	0.000	-2	792.667	0.972	-0.011
Annual		-0.681	-2.436	-22	950.000	0.496	-0.116

Trend detection of Mexico City, TRMM (1998-2017)						
Mann-Kendall Test & Sen's Slope						
Indicators	Z-Value	Sen's slope	S	Var(S)	P-value	Tau
Consecutive Wet Days (CWD)	-0.361	0.000	-12	929.333	0.718	-0.063
R10	1.433	0.394	45	942.333	0.152	0.237
R20	0.297	0.000	10	919.333	0.767	0.053
Total Rainfall (NOV-JAN)	1.071	0.665	34	950.000	0.284	0.179
Maximum Rainfall (NOV-JAN)	1.071	0.541	34	950.000	0.284	0.179
Total Rainfall (FEB-APR)	1.200	1.401	38	950.000	0.230	0.200
Maximum Rainfall (FEB-APR)	1.720*	1.003	54	950.000	0.086	0.284
Total Rainfall (MAY-JUL)	0.746	1.642	24	950.000	0.456	0.126

Trend detection of Mexico City, TRMM (1998-2017)						
Mann-Kendall Test & Sen's Slope						
Indicators	Z-Value	Sen's slope	S	Var(S)	P-value	Tau
Maximum Rainfall (MAY-JUL)	-0.552	-0.541	-18	950.000	0.581	-0.095
Total Rainfall (AUG-OCT)	-1.330	-3.668	-42	950.000	0.183	-0.221
Maximum Rainfall (AUG-OCT)	-0.941	-1.440	-30	950.000	0.347	-0.158
Total Rainfall in Wet Period (MAY-OCT)	-0.876	-4.374	-28	950.000	0.381	-0.147
Total Rainfall in Dry period (NOV-APR)	1.590	1.700	50	950.000	0.112	0.263
Maximum Rainfall in Wet Period (MAY-OCT)	-1.071	-1.906	-34	950.000	0.284	-0.179
Maximum Rainfall in Dry period (NOV-	1.784*	0.943	56	950.000	0.074	0.295

Trend detection of Mexico City, TRMM (1998-2017)						
Mann-Kendall Test & Sen's Slope						
Indicators	Z-Value	Sen's slope	S	Var(S)	P-value	Tau
APR)						

99% confidence interval (***), 95% confidence interval (**), 90% confidence interval (*)

Table 9: Mann Kendal Trend Analysis and Sen's Slope Analysis of Jakarta

Trend detection of station data of Jakarta (1979-2017)							
Mann-Kendall Test & Sen's Slope							
Indicators		Z-Value	Sen's slope	S	Var(S)	P-value	Tau
Monthly Total Rainfall	January	-0.121	-0.197	-11	6833.667	0.904	-0.015
	February	2.976***	4.420	247	6833.667	0.003	0.333
	March	1.210	0.858	101	6833.667	0.226	0.136
	April	0.750	0.638	63	6833.667	0.453	0.085
	May	0.677	0.570	57	6833.667	0.498	0.077
	June	1.573	1.064	131	6833.667	0.116	0.177

Trend detection of station data of Jakarta (1979-2017)							
Mann-Kendall Test & Sen's Slope							
Indicators		Z-Value	Sen's slope	S	Var(S)	P-value	Tau
	July	0.798	0.878	67	6833.667	0.425	0.090
	August	-0.992	-0.531	-83	6833.667	0.321	-0.112
	September	-0.871	-0.644	-73	6833.667	0.384	-0.099
	October	0.218	0.159	19	6833.667	0.828	0.026
	November	1.185	1.038	99	6833.667	0.236	0.134
	December	-1.331	-1.395	-111	6833.667	0.183	-0.150
Daily Maximum Rainfall	January	1.573	0.423	131	6833.667	0.116	0.177
	February	2.952***	0.909	245	6833.667	0.003	0.331
	March	1.355	0.227	113	6833.667	0.175	0.152
	April	0.121	0.027	11	6833.667	0.904	0.015
	May	1.234	0.203	103	6833.667	0.217	0.139
	June	1.766*	0.314	147	6833.667	0.077	0.198
	July	0.677	0.116	57	6833.667	0.498	0.077

Trend detection of station data of Jakarta (1979-2017)							
Mann-Kendall Test & Sen's Slope							
Indicators		Z-Value	Sen's slope	S	Var(S)	P-value	Tau
	August	-0.750	-0.128	-63	6833.667	0.453	-0.085
	September	-0.242	-0.082	-21	6833.667	0.809	-0.028
	October	-0.073	-0.008	-7	6833.667	0.942	-0.009
	November	0.024	0.011	3	6833.667	0.981	0.004
	December	1.089	0.280	91	6833.667	0.276	0.123
No. of Rainy days (Rainfall ≥ 1mm)	January	-0.085	0.000	-8	6778.667	0.932	-0.011
	February	1.515	0.074	125	6701.667	0.130	0.169
	March	0.365	0.000	31	6758.333	0.715	0.042
	April	1.034	0.054	86	6754.667	0.301	0.116
	May	0.707	0.029	59	6736.333	0.480	0.080
	June	0.194	0.000	17	6777.000	0.846	0.023
	July	0.461	0.048	39	6801.667	0.645	0.053
	August	-0.668	-0.056	-56	6788.667	0.504	-0.076

Trend detection of station data of Jakarta (1979-2017)							
Mann-Kendall Test & Sen's Slope							
Indicators		Z-Value	Sen's slope	S	Var(S)	P-value	Tau
	September	-0.703	-0.067	-59	6798.333	0.482	-0.080
	October	0.582	0.042	49	6794.333	0.560	0.066
	November	0.451	0.000	38	6737.333	0.652	0.051
	December	-0.558	-0.050	-47	6789.000	0.577	-0.063
Annual Rainfall		1.573	12.553	131	6833.667	0.116	0.177
Consecutive Wet Days (CWD)		1.410	0.091	117	6769.000	0.159	0.158
R10		0.788	0.200	66	6812.667	0.431	0.089
R20		1.297	0.182	108	6801.333	0.194	0.146
Total Rainfall (JAN-MAR)		2.468**	7.161	205	6833.667	0.014	0.277
Total Rainfall (APR-JUN)		1.210	2.217	101	6833.667	0.226	0.136

Trend detection of station data of Jakarta (1979-2017)						
Mann-Kendall Test & Sen's Slope						
Indicators	Z-Value	Sen's slope	S	Var(S)	P-value	Tau
Total Rainfall (JUL-SEP)	-0.290	-0.898	-25	6833.667	0.772	-0.034
Total Rainfall (OCT-DEC)	0.435	1.277	37	6833.667	0.663	0.050
Maximum Rainfall (JAN-MAR)	1.984*	4.406	165	6833.667	0.047	0.223
Maximum Rainfall (APR-JUN)	0.653	0.359	55	6833.667	0.514	0.074
Maximum Rainfall (JUL-SEP)	-0.145	-0.182	-13	6833.667	0.885	-0.018

Trend detection of station data of Jakarta (1979-2017)						
Mann-Kendall Test & Sen's Slope						
Indicators	Z-Value	Sen's slope	S	Var(S)	P-value	Tau
Maximum Rainfall (OCT-DEC)	-0.097	-0.077	-9	6833.667	0.923	-0.012
Total Rainfall in Wet Season (OCT-MAR)	2.516**	9.246	209	6833.667	0.012	0.282
Total Rainfall in Dry Season (APR-SEP)	0.508	1.952	43	6833.667	0.611	0.058
Maximum Rainfall in Wet Season (OCT-MAR)	1.645*	3.350	137	6833.667	0.100	0.185
Maximum Rainfall in Dry Season (APR-	1.161	0.839	97	6833.667	0.246	0.131

Trend detection of station data of Jakarta (1979-2017)						
Mann-Kendall Test & Sen's Slope						
Indicators	Z-Value	Sen's slope	S	Var(S)	P-value	Tau
SEP)						

99% confidence interval (***), 95% confidence interval (**), 90% confidence interval (*)

Table 10: Mann Kendal Trend Analysis and Sen's Slope Analysis of Dhaka

Trend detection of BMD station data of Dhaka (1953-2017)							
Mann-Kendall Test & Sen's Slope							
Indicators		Z-Value	Sen's slope	S	Var(S)	P-value	Tau
Monthly Total Rainfall	January	-0.255	0.000	-42	25947.333	0.799	-0.021
	February	0.332	0.000	58	29532.000	0.740	0.029
	March	1.179	0.233	204	29656.000	0.238	0.101
	April	0.348	0.240	61	29785.000	0.728	0.030
	May	-0.336	-0.240	-59	29782.333	0.737	-0.029
	June	-0.829	-0.734	-144	29790.000	0.407	-0.071

Trend detection of BMD station data of Dhaka (1953-2017)							
Mann-Kendall Test & Sen's Slope							
Indicators		Z-Value	Sen's slope	S	Var(S)	P-value	Tau
Daily Maximum Rainfall	July	0.295	0.362	52	29790.000	0.768	0.026
	August	0.220	0.140	39	29784.333	0.826	0.019
	September	0.267	0.214	47	29789.000	0.790	0.023
	October	0.238	0.171	42	29785.333	0.812	0.021
	November	-0.843	0.000	-143	28349.667	0.399	-0.071
	December	0.701	0.000	106	22418.667	0.483	0.053
	January	-0.267	0.000	-44	25950.000	0.790	-0.022
	February	-0.151	0.000	-27	29507.667	0.880	-0.013
	March	1.185	0.141	205	29633.667	0.236	0.102
	April	0.157	0.009	28	29758.000	0.876	0.014
	May	-0.151	-0.018	-27	29760.333	0.880	-0.013
	June	-0.852	-0.200	-148	29768.000	0.394	-0.073
	July	-0.875	-0.213	-152	29770.667	0.381	-0.075

Trend detection of BMD station data of Dhaka (1953-2017)							
Mann-Kendall Test & Sen's Slope							
Indicators		Z-Value	Sen's slope	S	Var(S)	P-value	Tau
	August	-0.568	-0.147	-99	29781.000	0.570	-0.049
	September	-0.435	-0.122	-76	29777.333	0.664	-0.038
	October	0.713	0.141	124	29772.000	0.476	0.062
	November	-0.778	0.000	-132	28346.667	0.437	-0.065
	December	0.701	0.000	106	22419.333	0.483	0.053
No. of Rainy days (Rainfall ≥ 1mm)	January	-0.234	0.000	-37	23623.667	0.815	-0.018
	February	0.708	0.000	120	28246.667	0.479	0.060
	March	0.750	0.000	129	29127.000	0.453	0.064
	April	0.782	0.000	135	29381.000	0.434	0.067
	May	1.027	0.000	177	29345.000	0.304	0.088
	June	-2.978***	-0.063	-512	29452.000	0.003	-0.254
	July	0.397	0.000	69	29311.667	0.691	0.034
	August	-1.152	0.000	-198	29240.667	0.249	-0.098

Trend detection of BMD station data of Dhaka (1953-2017)							
Mann-Kendall Test & Sen's Slope							
Indicators		Z-Value	Sen's slope	S	Var(S)	P-value	Tau
	September	1.055	0.020	182	29433.333	0.291	0.090
	October	-0.625	0.000	-108	29294.667	0.532	-0.054
	November	-0.678	0.000	-113	27254.333	0.498	-0.056
	December	0.428	0.000	63	21019.667	0.669	0.031
Annual Rainfall		-0.145	-0.521	-26	29790.000	0.885	-0.013
Consecutive Wet Days (CWD)		-1.489	-0.043	-257	29562.333	0.137	-0.127
R10		0.824	0.058	143	29709.667	0.410	0.071
R20		0.522	0.022	91	29670.333	0.601	0.045
Total Rainfall (DEC-FEB)		0.371	0.036	65	29729.667	0.711	0.032
Maximum Rainfall (DEC-FEB)		0.522	0.057	91	29721.667	0.602	0.045

Trend detection of BMD station data of Dhaka (1953-2017)						
Mann-Kendall Test & Sen's Slope						
Indicators	Z-Value	Sen's slope	S	Var(S)	P-value	Tau
Total Rainfall (MAR-MAY)	0.232	0.308	41	29787.000	0.817	0.020
Maximum Rainfall (MAR-MAY)	-0.180	-0.106	-32	29783.333	0.857	-0.016
Total Rainfall (JUN-SEP)	-0.214	-0.768	-38	29792.000	0.830	-0.019
Maximum Rainfall (JUN-SEP)	-0.689	-0.875	-120	29788.000	0.491	-0.060
Total Rainfall (OCT-NOV)	0.029	0.025	6	29790.000	0.977	0.003
Maximum Rainfall (OCT-	0.023	0.000	5	29781.667	0.982	0.002

Trend detection of BMD station data of Dhaka (1953-2017)						
Mann-Kendall Test & Sen's Slope						
Indicators	Z-Value	Sen's slope	S	Var(S)	P-value	Tau
NOV)						
Total Rainfall in WET Season (MAY-OCT)	-0.504	-1.306	-88	29788.000	0.614	-0.044
Maximum Rainfall in WET Season (MAY-OCT)	-0.904	-0.942	-157	29789.000	0.366	-0.078
Total Rainfall in DRY Season(NOV-APR)	0.423	0.338	74	29786.000	0.672	0.037

Trend detection of BMD station data of Dhaka (1953-2017)						
Mann-Kendall Test & Sen's Slope						
Indicators	Z-Value	Sen's slope	S	Var(S)	P-value	Tau
Maximum Rainfall in DRY Season(NOV-APR)	0.267	0.163	47	29783.000	0.790	0.023

99% confidence interval (***), 95% confidence interval (**), 90% confidence interval (*)

(ii) SPI Calculation

For urban floods, we only consider SPI values for 1 month periods with values greater than 1, as -0.99<SPI<0.99 is near normal and negative values are typically considered for drought scenarios. Here, all the graphs are created for 1 month SPI to determine the soil moisture condition conducive to urban flooding. In the SPI graphs for Houston, it is clear that SPI values higher than 2, which indicates extremely wet conditions, are not frequent. Most of the SPI values are below 1 with some exceptional months. Year 1992, 1994, 1998, 2001, 2003, 2015 and 2017 are some of the flood years of Houston, which justifies their high SPI value. For Mexico City, only 4-5 months SPI values crossed 2. Moderately wet and very wet conditions are not recurrent. In Jakarta, SPI values greater than 1 are observed since 2007 (2007, 2010,

2012, 2013, 2017), which ranges from moderately wet to very wet. Extreme wet conditions are very few for Jakarta. For Dhaka, moderately wet to very wet condition is frequent since 1956. Extremely wet condition for Dhaka is observed very occasionally. The SPI graphs for all study areas are represented in Figure 3.

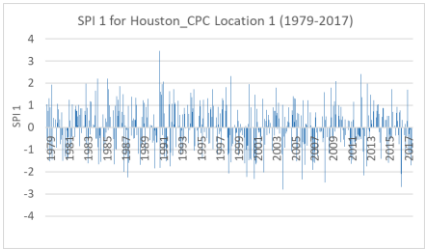

(A) SPI graph for Houston in Location 1 of CPC gauge

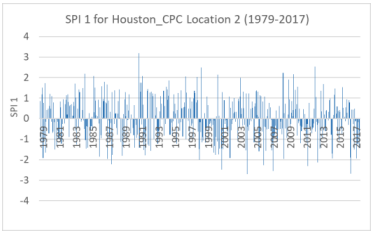

(B) SPI graph for Houston in Location 2 of CPC gauge

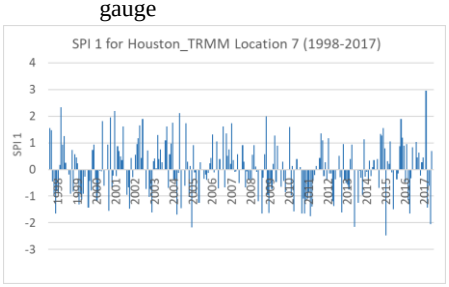

(C) SPI graph for Houston in Location 7 of TRMM gauge

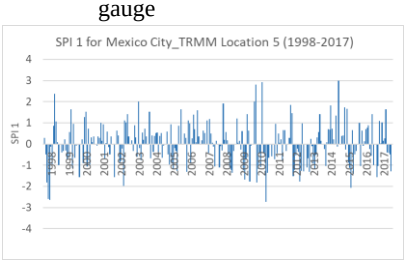

(D) SPI graph for Mexico City in Location 5 of TRMM gauge

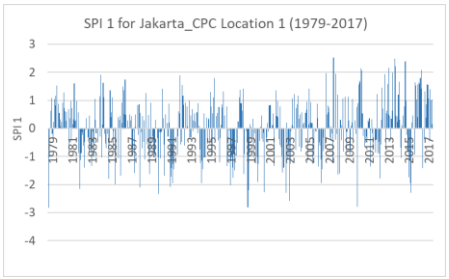

(E) SPI graph for Jakarta in Location 1 of CPC gauge

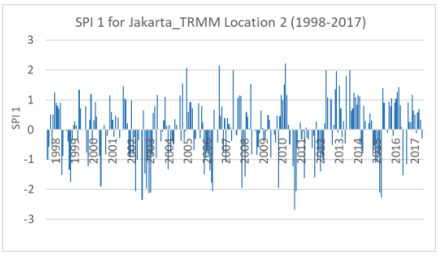

(F) SPI graph for Jakarta in Location 2 of TRMM gauge

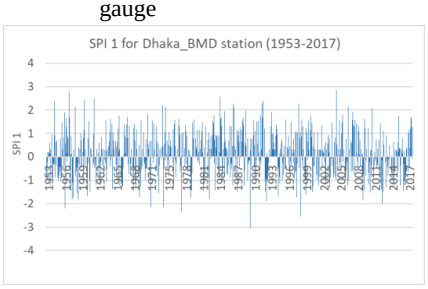

(G) SPI graph for Dhaka in Location 1 of BMD gauge

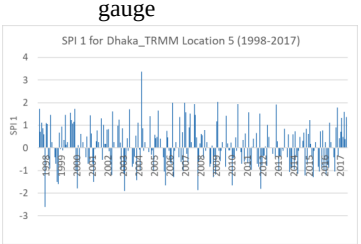

(H) SPI graph for Dhaka in Location 5 of TRMM gauge

Figure 3: Standardized Precipitation Index (SPI) graphs for different megacities

Validation of the LULC Analysis

The validation of the LULC analysis for Houston for year 2007 is done using 2006 National Land Cover Dataset (NLCD). The comparison of the total area and percentage is given below.

Table 11: Validation of LULC Analysis for Houston

Houston 2007	Area (acres)	Percentage	Houston2006 (NLCD)	Area (acres)	Percentage
Barren Land	53,843	5.98	Barren Land + Herbaceous	32364	3.41
Forest Land	267,997	29.78	Deciduous Forest + Evergreen Forest + Mixed Forest + Shrub/Scrub	149491	15.76
Urban Area	348,966	38.78	Developed Low Intensity + Developed Medium Intensity + Developed High Intensity	471023	49.64
Vegetative Cover	201,341	22.38	Hay/Pasture + Cultivated Crops + Woody Wetlands + Developed Open Space	273435	28.82
Water	15,286	1.70	Open Water	14392	1.52
Sand Filling	12,402	1.38	Wetlands	8116	0.86
Future Housing Projects		–			–
Total	899,835	100.00	Total	948822	100.00

Urban Flood Risk Maps

The risk index calculated from equation (9) are subdivided into 5 classes. The risk index value ranges from -21 to 21. Any area is considered in no risk zone if the index value is negative or zero, as we are considering urban flood here. Other classes are: low risk (0.01-6), moderate risk (6.01-12), high risk (12.01-18) and extreme risk (18.01-21). Figure 4 represents the urban flood risk of study area for specific month and year.

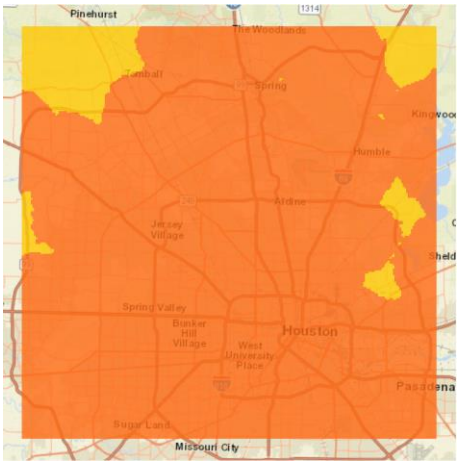

(i) Houston, August 2007

(ii) Houston, August 2017

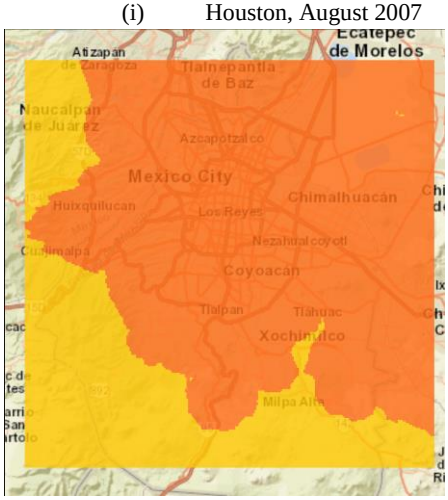

(iii) Mexico City, August 2007

(iv) Mexico City, August 2017

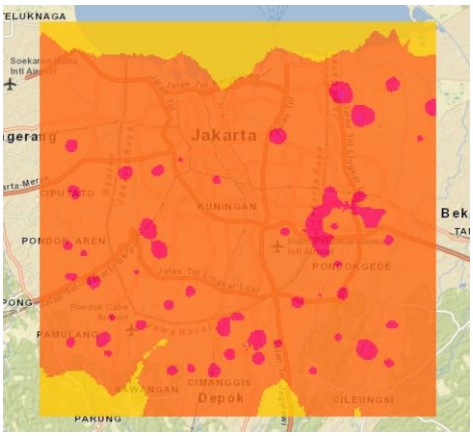

(v) Jakarta, December 2007

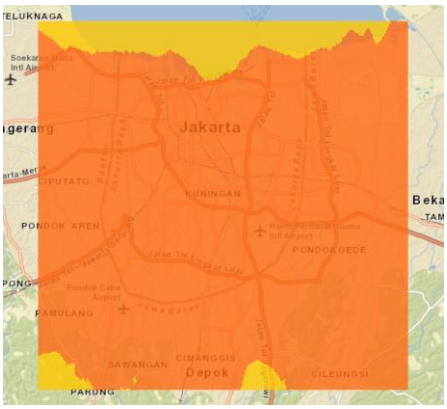

(vi) Jakarta, December 2017

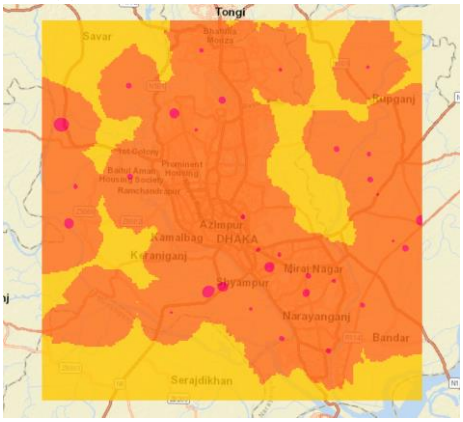

(vii) Dhaka, July 2007

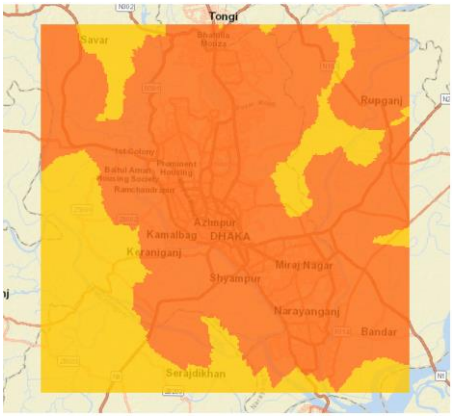

(viii)Dhaka, July 2017

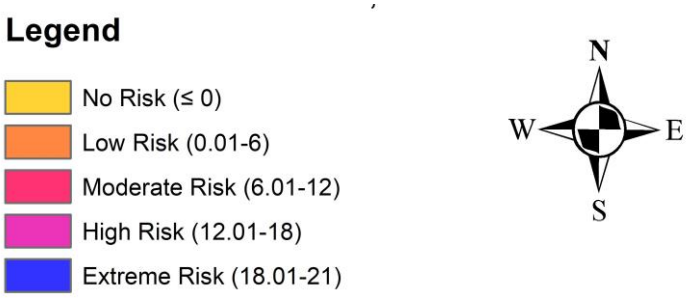

Figure 4: Urban Flood risk map of different wet season months of each study area to compare the change of risk between the year 2007 and year 2017

Validation of Urban Flood Risk Map with Federal Emergency Management Agency (FEMA) Flood Hazard layer

In our risk index calculation, we took LULC change and rainfall components only. Land elevation is another important factor that needs to be considered while calculating the urban flood risk index. For validating the urban flood risk map, we overlaid the map on the Federal Emergency Management Agency (FEMA) flood hazard layer for Houston. For better visualization, only a part of Houston is focused in Figure 5. FEMA updates their flood hazard data through Flood Insurance Rate Maps (FIRMs) (Xian, Lin, & Hatzikyriakou, 2015). FIRMs demarcate flood risk zones using hydrological and topographic survey outputs (Xian et al., 2015). The high risk and moderate risk areas of the urban flood risk maps match with 1% annual chance flood hazard, floodway, and 0.2% annual chance flood hazard area in most of the places with some exceptions. 1% annual chance flood hazard areas are defined as the areas that are situated on 100-year flood zones (Grineski, Collins, Chakraborty, & Montgomery, 2015). The FEMA flood map does not provide information on actual flood events but the probability of flooding (Grineski et al., 2015). A qualitative check on the two maps shows partial validation of our risk calculation approach, while there is room for improvement for areas that are prone to flooding due to distinct elevation changes such as rivers, streams, and bayous.

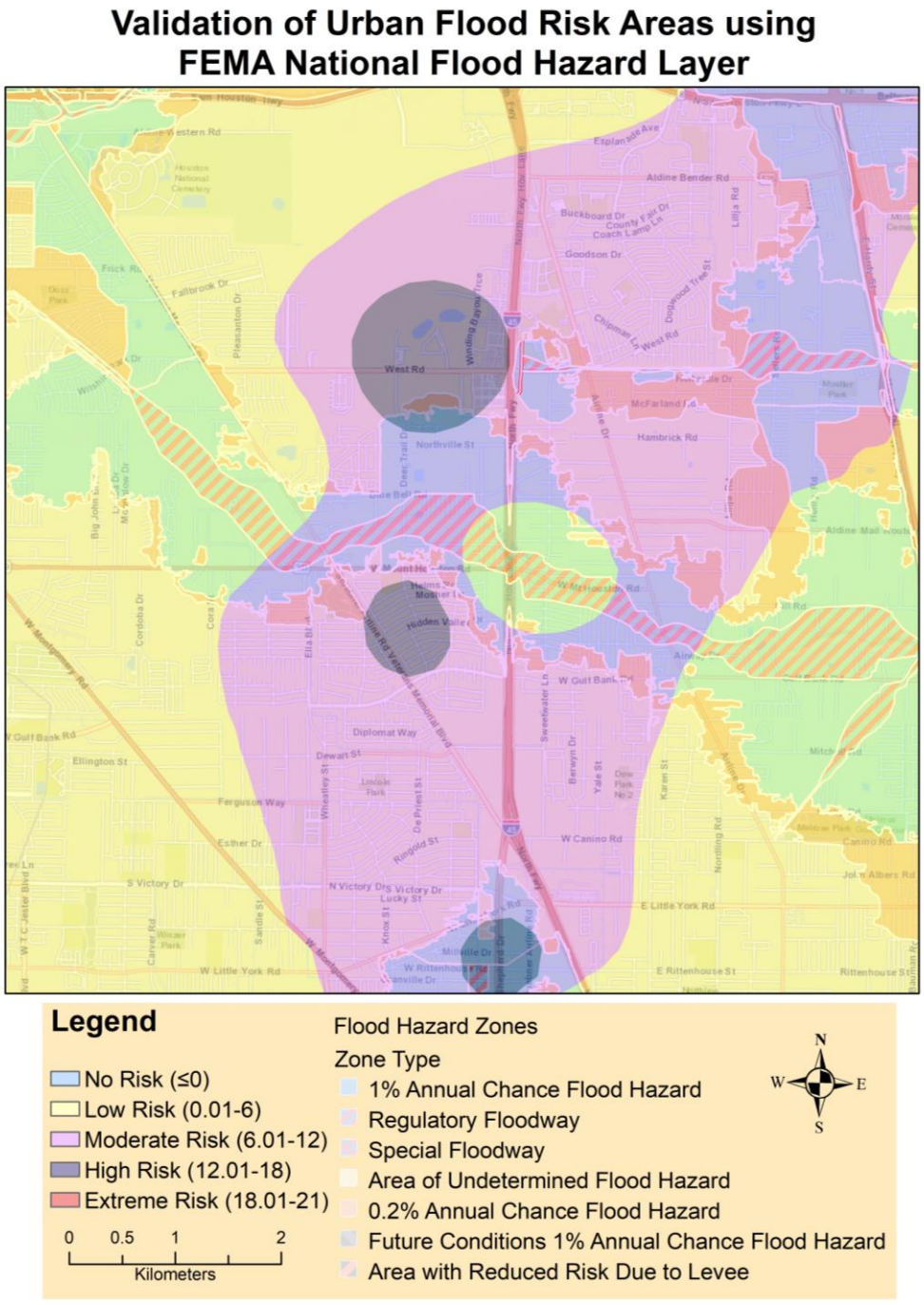

Figure 5: Validation of Urban Flood risk map of Houston with FEMA flood hazard layer

4 Discussions and Conclusion

With the expansion of urbanization, vegetated soils convert to impervious surfaces that increase storm water flow and decrease both infiltration and natural storage (Wheater & Evans, 2009). Higher vegetative cover facilitates higher infiltration rate and quantity (Loch, 2000). The rate and magnitude of infiltration are dependent on the type, duration and intensity of precipitation, initial soil moisture content, soil type, evaporation, vegetation coverage, and terrain slope (G. Zhang, Qian, Wang, & Zhao, 2014). The soil composition of Houston is mainly the combination of fine sandy loam and clay, which has poor draining capacity (Muñoz, Olivera, Giglio, & Berke, 2018). Like Houston, the soil profile of Central Jakarta consists of alluvial clay in the form of soft to stiff (Hsiung, Yang, Aila, & Ge, 2018) and Dhaka city is a blend of Pleistocene clayey soils and Holocene clayey and sandy soils (Rahman, Kamal, & Siddiqua, 2018). As infiltration capacity of the clayey soil is less than that of sandy soil due to its smaller pore size, it is understood to be one of the main reasons that cause urban flooding in our study areas. In addition, rain on barren land compacts the upper layer of soil, creating hindrance in infiltration and causing excess runoff. Therefore, increasing amount of barren lands in these megacities are also responsible for urban flooding. According to Manning's equation, the velocity of the storm water flow is indirectly proportional with the roughness of the land surface (Leopold, Wolman, & Miller, 2012). Therefore, increasing paved smooth surfaces amplify the storm water flow more than any natural rough surface (Jacobson, 2011). Also, higher soil moisture has less ability to absorb extra runoff after precipitation. After analyzing the SPI graphs, it becomes clear that urban flooding is occurring despite of having low SPI

values, where low value indicates that the soil moisture is not high to be considered extremely wet. Rather, the values are indicating nearly normal to moderately wet soil moisture condition except some exceptional months.

Absence of zoning ordinance in Houston enables unplanned rapid increase of urban areas (Lynn, 2017). However, planners and developers have enough room to provide plans that can maximize urban and suburban vegetation within any development project (Conlon, Monaghan, Hayden, & Wilhelmi, 2016). The flat topography adds more difficulty in the flooding situation. Apart from planners, communities have started working on sustainable solution by changing unused golf courses to detention basins in the southeastern part of Houston to accommodate extra water after heavy precipitation (Landers, 2017). As reducing impervious layer is not easy inside cities, Low Impact Development (LID) practices can be helpful in reducing the excess runoff. These practices are used to manage storm water at the source by providing permeable pavements, bio-retention areas, and creating intermittent impervious surface (Damodaram et al., 2010). These could be potential remedies to decrease the heavy runoff due to impervious layers.

Due to the combined sewer system in Mexico City, volume of wastewater after heavy rainfall increases immensely. In base flow conditions, the waste water volume is 45 m^3/s, which increases to 300 m^3/s in peak flow conditions (Siemens, Huschek, Siebe, & Kaupenjohann, 2008). The pipe network of the combined sewer system is complex due to large difference in pipe diameter (0.30 m to 3.05 m). The system also generates sediment (Jiménez, Méndez, Barrios, Salgado, & Sheinbaum, 2004), which hampers the flow and creates more flood risk eventually for the city. The authority

extracts 0.85 Mm^3 of sediments (Jiménez et al., 2004) from the system every year and disposes as landfill, but cannot cope with the heavy rate of sedimentation in combined sewers.

Imprudent storm water drainage (Padawangi & Douglass, 2015) of Jakarta is another reason that is responsible for repetitive flood occurrence. Besides, insufficient finances to develop institutional capabilities, regulatory framework is also responsible for this situation (Kartez & Lindell, 1987). Changes of land ownership and extensive land development projects have influence on urban flooding (Walker, Whittle, Medd, & Walker, 2011). East flood canal project, the World Bank funded project named Jakarta Urgent Flood Mitigation Project / Jakarta Emergency Dredging Initiative (JUFMP/JEDI), proposed sea wall project is expected to be helpful in decreasing the flood risk in urban Jakarta (Padawangi & Douglass, 2015).

Apart from natural factors, stormwater management of these cities is also responsible for the situation. For example, Dhaka has only 30% and 38% coverage of sewerage and storm water systems, respectively (World Bank: BD: Dhaka Water Supply & Sanitation Project, 2017). Many areas of Dhaka have local combined sewer facilities, which cannot accommodate the excess runoff due to high-intensity precipitation. Surface runoff goes to underground sewer networks through catch pits. Inadequate intake capacity of catch pits or insufficient drainage capacity of sewer pipes cause surface flooding, which can contribute to urban flooding (Mark, Apirumanekul, Kamal, & Praydal, 2001).

The result of the study shows strong evidence that land use and land cover change (LULC) and insufficient water and drainage infrastructure development is mostly

accountable for urban flooding with moderate impact from precipitation alteration. Urban flood can occur any time but the frequency of occurrence is higher in wet periods of any area. The rainfall trends in wet periods of Houston, Mexico City and Dhaka are negative and for Jakarta, it is positive. It implies that land use land cover change is the main driving factor behind urban flooding in Houston, Mexico City, and Dhaka. For Jakarta, both factors are equally important for urban flooding.

Before approving any area as urban area, planners should test soil characteristics, which play a vital role in infiltrating floodwater and excess runoff. Accuracy metrics for LULC change analysis should be added in future analysis. In addition to protecting as much land as possible to preserve natural hydrological and drainage characteristics, installation of high capacity pumping stations, accommodating Low Impact Development (LID) practices should be incorporated at planning and implementation levels. Natural canal excavation to increase capacity, reclaiming illegally filled canals, separate sewage and storm water drainage system, and provision of retention basins and rainwater harvesting can further reduce the intensity of urban flooding conditions in developing cities. Strict law enforcement is also required in order to track and stop the illegal landfilling of the natural drainage system. Proper zoning is necessary to stop haphazard urbanization. As the world is rapidly urbanizing, steps to identify and reduce urban flooding disasters with the assistance of Earth Observations based analysis in the fastest growing megacities should be encouraged and adopted.

Appendix I: Map of Unsupervised Image Classification of the study areas

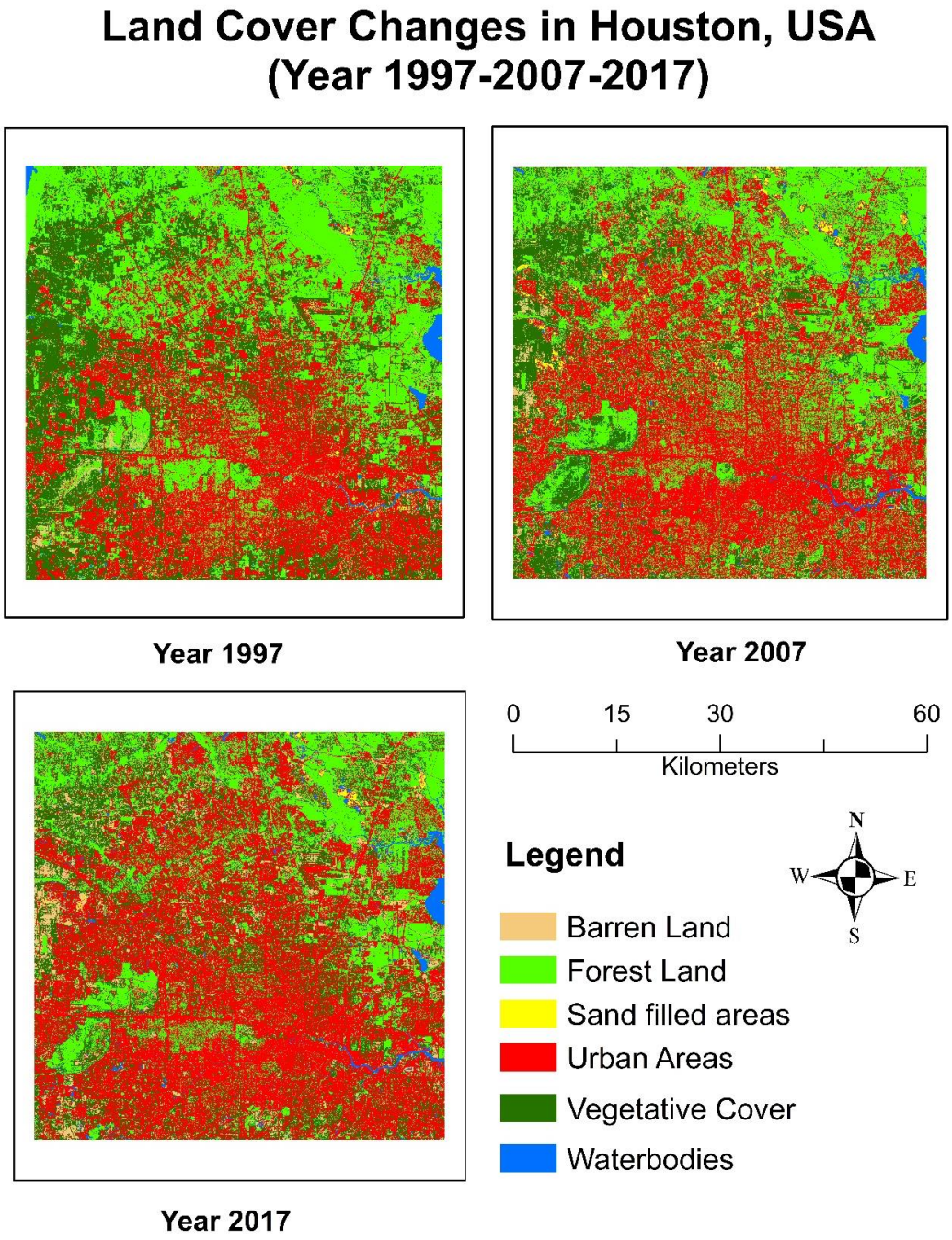

Figure: Land Cover changes in Houston, USA

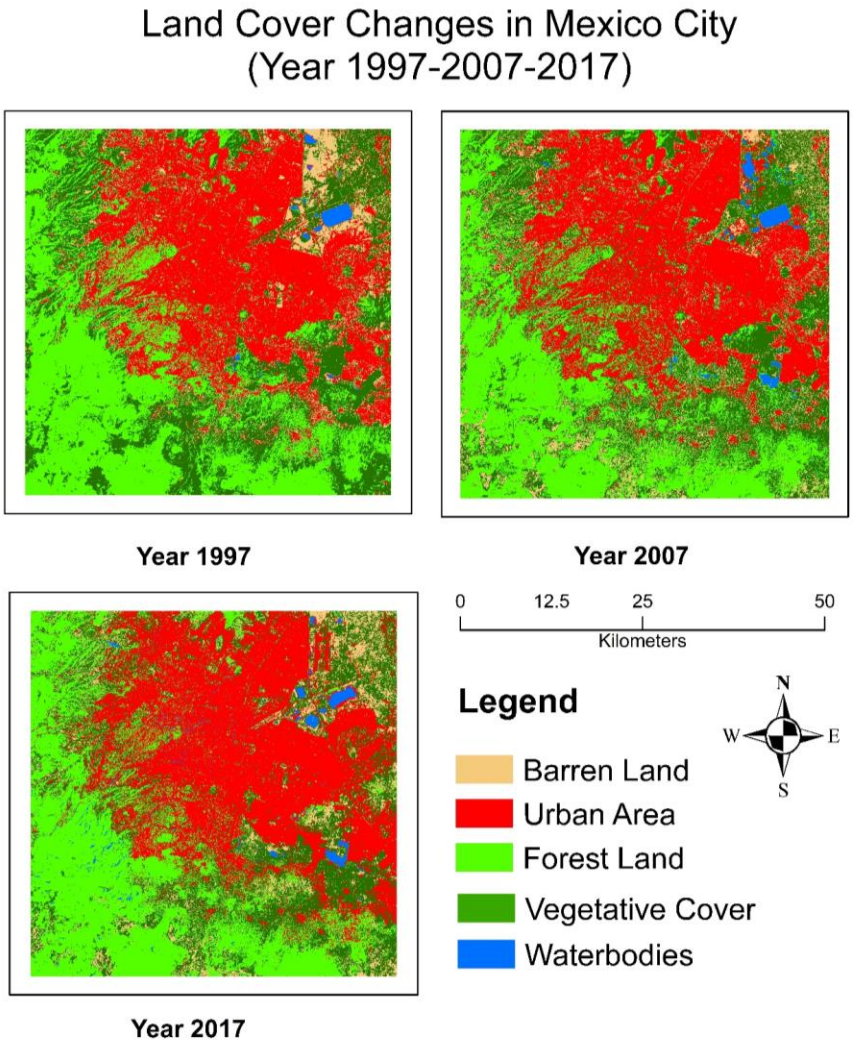

Figure: Land Cover changes in Mexico City, Mexico

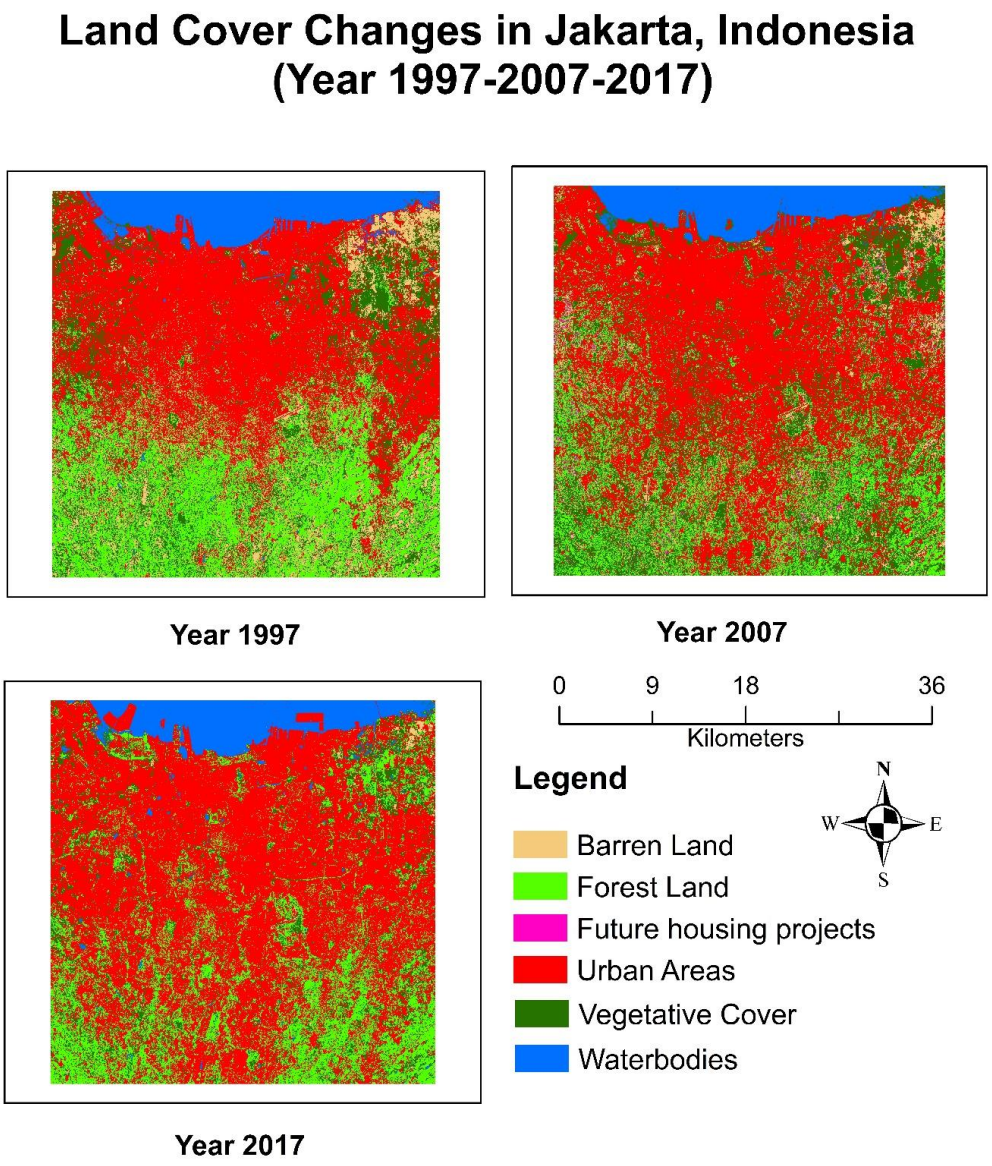

Figure: Land Cover changes in Jakarta, Indonesia

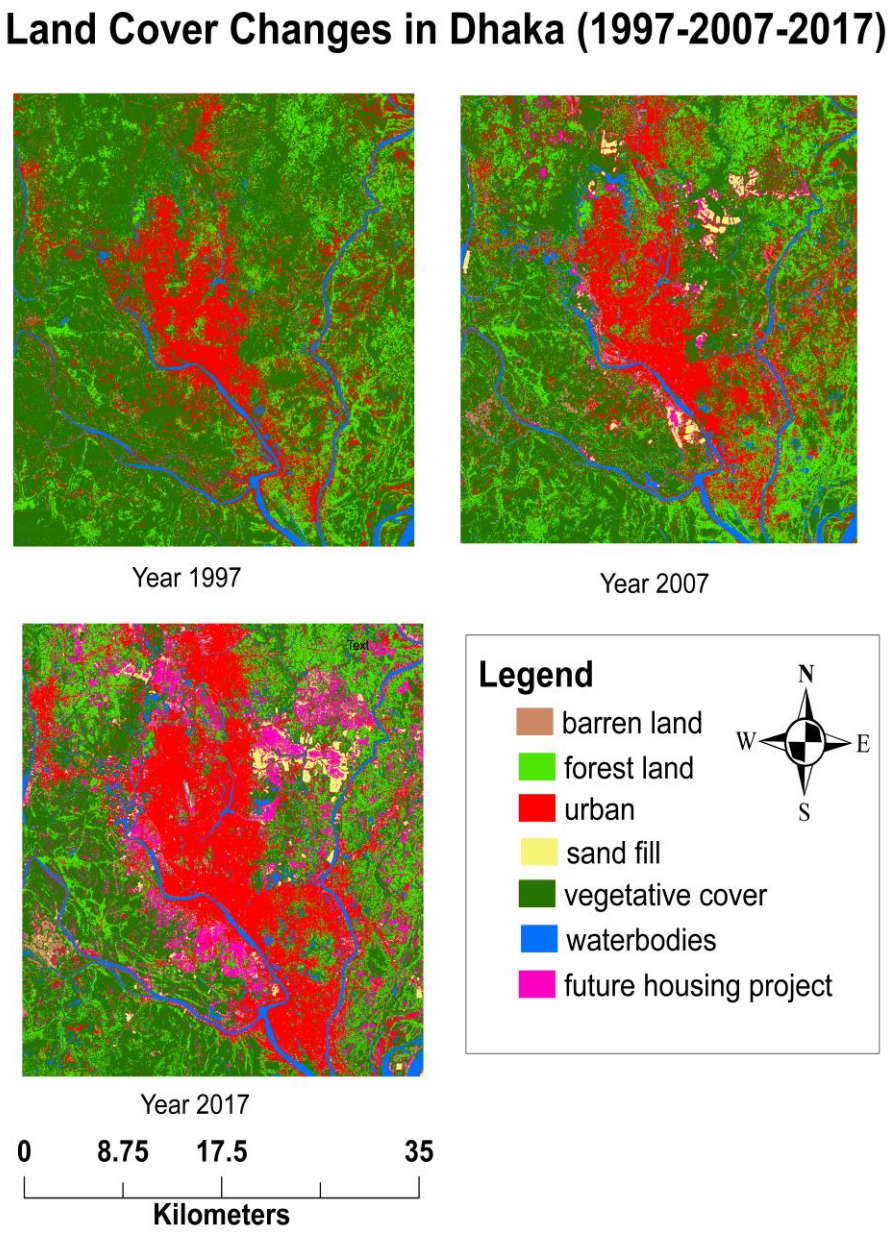

Figure: Land Cover changes in Dhaka, Bangladesh

Appendix II: Post-classification land-cover change detection of the study areas

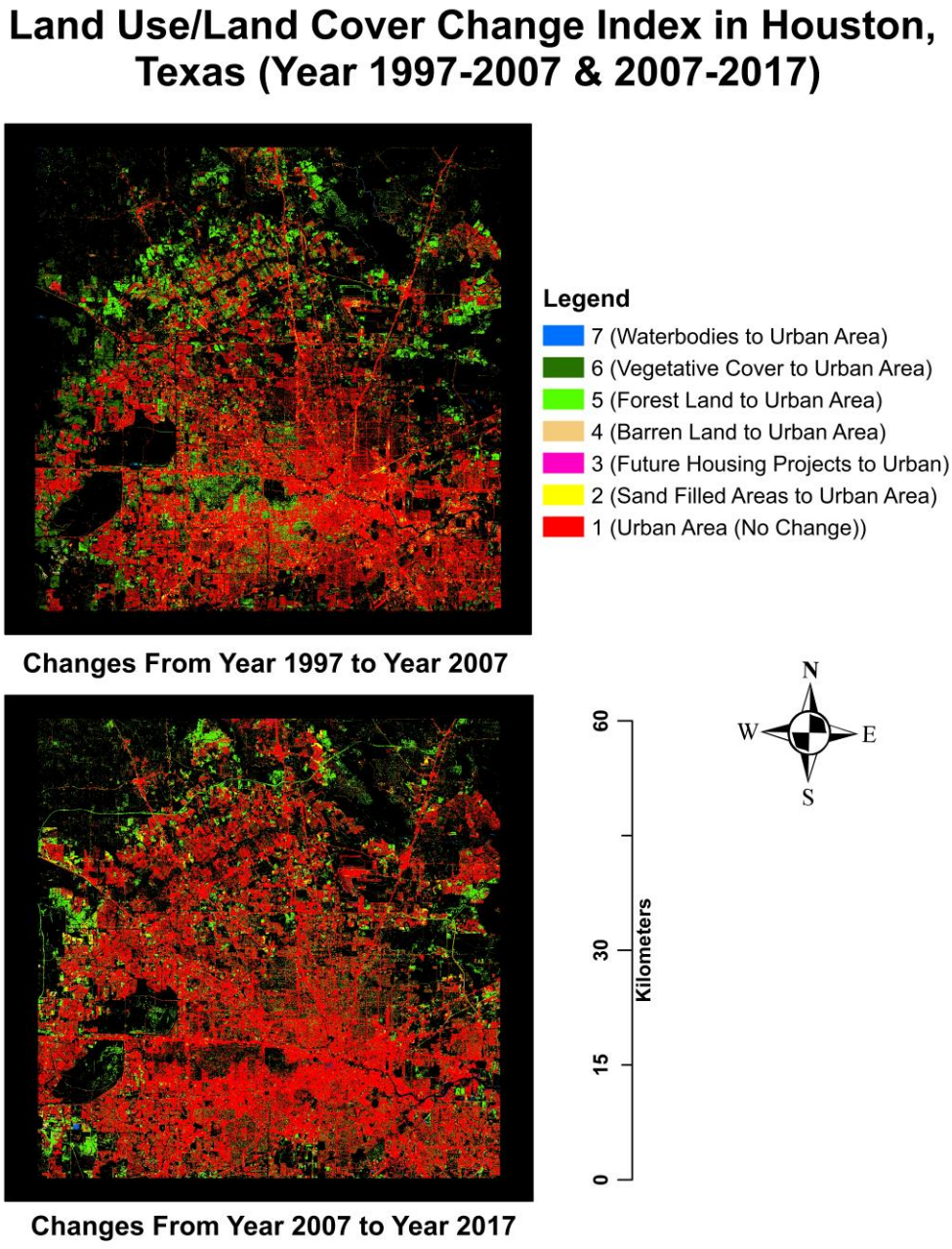

Land Use/Land Cover Change Index in Mexico City, Mexico (Year 1997-2007 & 2007-2017)

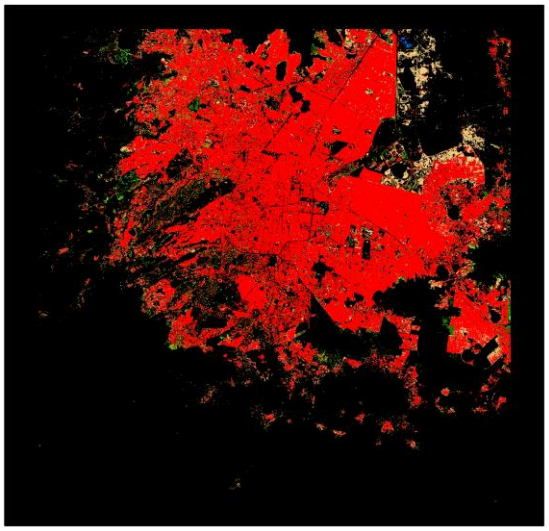

Changes From Year 1997 to Year 2007

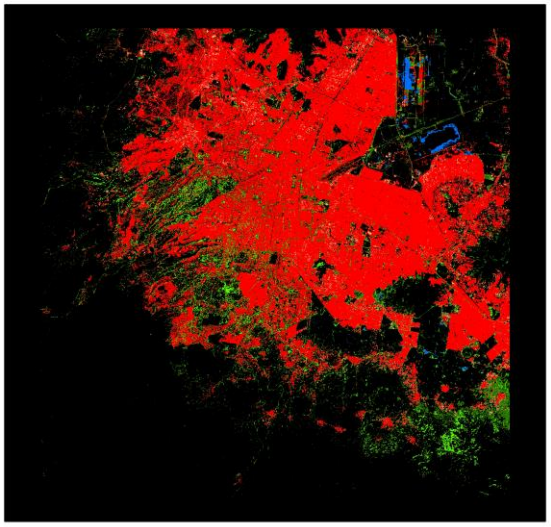

Changes From Year 2007 to Year 2017

Legend

- 7 (Waterbodies to Urban Area)
- 6 (Vegetative Cover to Urban Area)
- 5 (Forest Land to Urban Area)
- 4 (Barren Land to Urban Area)
- 3 (Future Housing Projects to Urban)
- 2 (Sand Filled Areas to Urban Area)
- 1 (Urban Area (No Change))

N
W E
S

0 12.5 25 50
Kilometers

Land Use/Land Cover Change Index in Jakarta, Indonesia (Year 1997-2007 & 2007-2017)

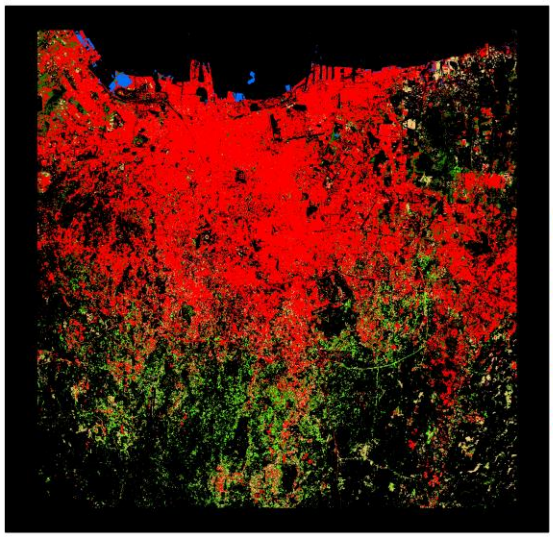

Changes From Year 1997 to Year 2007

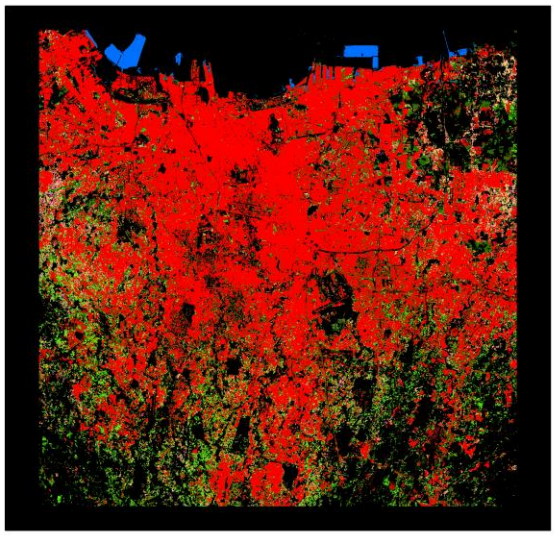

Changes From Year 2007 to Year 2017

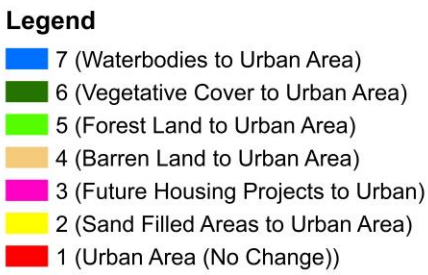

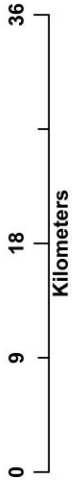

Land Use/Land Cover Change Index in Dhaka (Year 1997-2007 & 2007-2017)

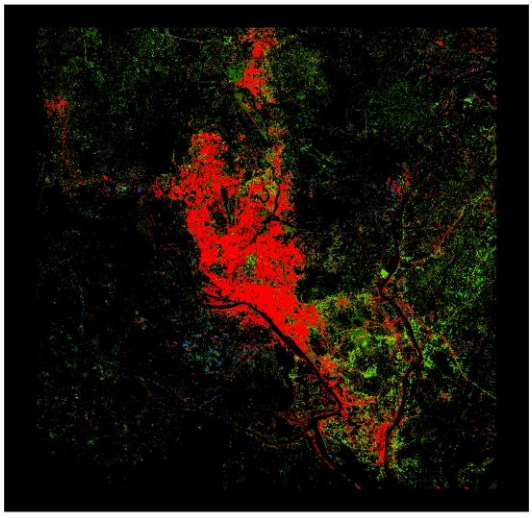

Legend

- 7 (Waterbodies to Urban Area)
- 6 (Vegetative Cover to Urban Area)
- 5 (Forest Land to Urban Area)
- 4 (Barren Land to Urban Area)
- 3 (Future Housing Projects to Urban)
- 2 (Sand Filled Areas to Urban Area)
- 1 (Urban Area (No Change))

Changes From Year 1997 to Year 2007

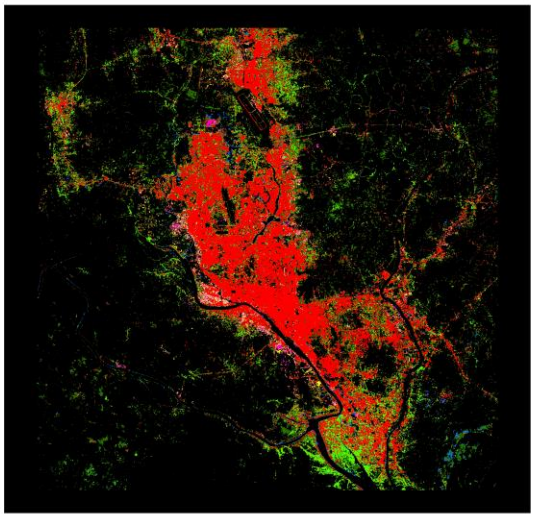

Changes From Year 2007 to Year 2017

Appendix III: Transformation of different land use/ land covers to urban areas

Land Use/Land Cover changed to Urban Area	Houston				Mexico City			
	year 1997 to 2007	Percentage	year 2007 to 2017	Percentage	year 1997 to 2007	Percentage	year 2007 to 2017	Percentage
barren land to urban	8,707.88	6.15	19,342.10	16.07	19,440.23	55.74	12,157.67	22.38
forest land to urban	64,048.87	45.21	53,895.66	44.77	5,796.95	16.62	18,400.74	33.87
urban area (no change)	207,286.17	0.00	284,848.77	0.00	170,949.90	0.00	178,305.75	328.22
vegetative cover to urban	56,029.96	39.55	38,263.96	31.78	9,527.40	27.32	21,930.36	40.37
waterbodies to urban	530.63	0.37	1,474.04	1.22	112.53	0.32	1,836.98	3.38
sand filled area to urban	12,362.06	8.73	7,413.98	6.16	-	0.00	-	0.00
future housing projects to urban	-	0.00	-	0.00	-	0.00	-	0.00
total area (urban not included)	141,679.41		120,389.74		34,877.11		54,325.75	

Land Use/Land Cover changed to Urban Area	Jakarta				Dhaka			
	year 1997 to 2007	Percentage	year 2007 to 2017	Percentage	year 1997 to 2007	Percentage	year 2007 to 2017	Percentage
barren land to urban	15,176.23	31.51	10,529.74	15.32	1,348.60	3.54	3,357.27	8.28
forest land to urban	11,573.89	24.03	20,188.35	29.37	9,222.72	24.21	14,111.64	34.80
urban area (no change)	110,970.56	0.00	141,308.13	0.00	27,863.41	0.00	39,985.73	0.00
vegetative cover to urban	20,269.97	42.08	32,152.75	46.78	25,767.58	67.64	19,908.57	49.10
waterbodies to urban	1,146.45	2.38	2,547.09	3.71	1,756.47	4.61	1,608.58	3.97
sand filled area to urban	-	0.00	-	0.00	-	0.00	414.77	1.02
future housing projects to urban	-	0.00	3,317.02	4.83	-	0.00	1,146.00	2.83
total area (urban not included)	48,166.53		68,734.95		38,095.37		40,546.83	

Appendix IV: Specifications of Landsat TM and OLI images

Satellite	Sensor	Path /Row	Acquisition Date	Resolution (m)	Wavelength (μm) of the stacked Spectral Bands	Useful for Mapping
Landsat 5 (1984–2012)	Thematic Mapper (TM)	137/44	January 26, 1997	30	Blue (Band 1: 0.45–0.52)	Bathymetric mapping, distinguishing soil from vegetation, and deciduous from coniferous vegetation(Hugh-Jones, 1989)
					Green (Band 2: 0.52–0.60)	Emphasizes peak vegetation, which is useful for assessing plant vigor
					Red (Band 3: 0.63–0.69)	Discriminates vegetation slopes
			January 22, 2007		Near-infrared (Band 4: 0.76–0.90)	Emphasizes biomass content and shorelines
					Shortwave-infrared 1 (Band 5: 1.55–1.75)	Discriminates moisture content of soil and vegetation; penetrates thin clouds
Landsat 8 OLI / TIRS (2013–Now) (Gorelick et al., 2017)	OLI_TIRS	137/44	January 17, 2017	30	Blue (Band 2: 0.452–0.512)	Bathymetric mapping, distinguishing soil from vegetation, and deciduous from coniferous vegetation
					Green (Band 3: 0.533–0.590)	Emphasizes peak vegetation, which is useful for assessing plant vigor
					Red (Band 4: 0.636–0.673)	Discriminates vegetation slopes
					Near-infrared (Band 5: 0.851–0.879)	Emphasizes biomass content and shorelines

					Shortwave-infrared 1 (Band 6: 1.566–1.651)	Discriminates moisture content of soil and vegetation; penetrates thin clouds

(Pal & Ziaul, 2017)

Appendix V: Location of the TRMM stations and CPC gauges for all study areas

Houston TRMM Locations and CPC gauge Locations				Mexico City TRMM Locations and CPC gauge Location			
	Location	Latitude	Longitude		Location	Latitude	Longitude
	Location 1	29.625	-95.875		Location 1	19.125	-99.375
	Location 2	29.625	-95.625		Location 2	19.125	-99.125
	Location 3	29.625	-95.375		Location 3	19.125	-98.875
	Location 4	29.625	-95.125		Location 4	19.375	-99.375
	Location 5	29.875	-95.875		Location 5	19.375	-99.125
	Location 6	29.875	-95.625		Location 6	19.375	-98.875
	Location 7	29.875	-95.375		Location 7	19.625	-99.375
	Location 8	29.875	-95.125		Location 8	19.625	-99.125
	Location 9	30.125	-95.875		Location 9	19.625	-98.875
	Location 10	30.125	-95.625				
	Location 11	30.125	-95.375				
	Location 12	30.125	-95.125				
	Houston CPC gauge Location 1	29.75	-95.25				
	Houston CPC gauge Location 2	29.75	-95.75		Mexico City CPC gauge Location 1	19.25	-99.25

Jakarta TRMM Locations and CPC gauge Locations				Dhaka TRMM Locations and CPC gauge Locations			
	location 1	-6.375	106.625		location 1	23.625	90.125
	location 2	-6.375	106.875		location 2	23.625	90.375
	location 3	-6.375	107.125		location 3	23.625	90.625
	location 4	-6.125	106.625		location 4	23.875	90.125
	location 5	-6.125	106.875		location 5	23.875	90.375
	location 6	-6.125	107.125		location 6	23.875	90.375
	Jakarta CPC gauge Location 1	-6.25	106.75		Dhaka BMD gauge Location 1	23.75	90.25

Appendix VI: Standardized Precipitation Index Graphs

Standardized Precipitation Index Graphs for Houston

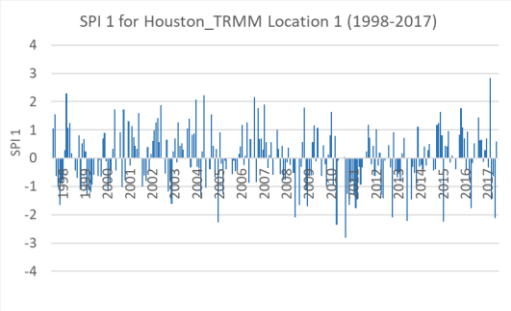

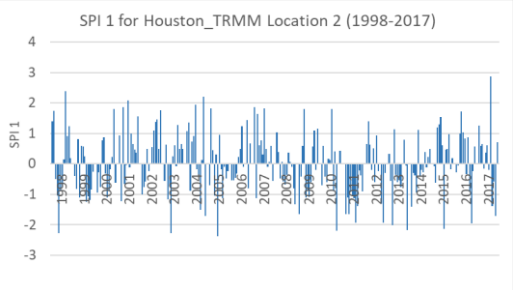

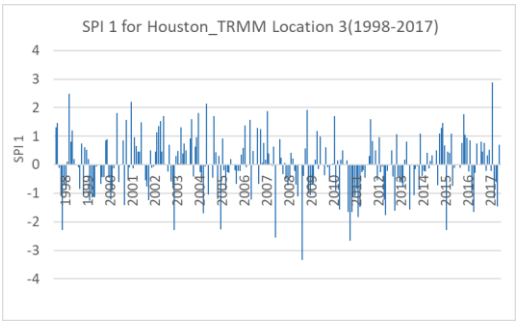
SPI 1 for Houston_TRMM Location 3(1998-2017)
SPI 1

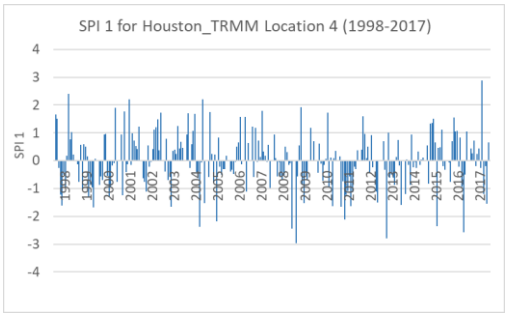
SPI 1 for Houston_TRMM Location 4 (1998-2017)
SPI 1

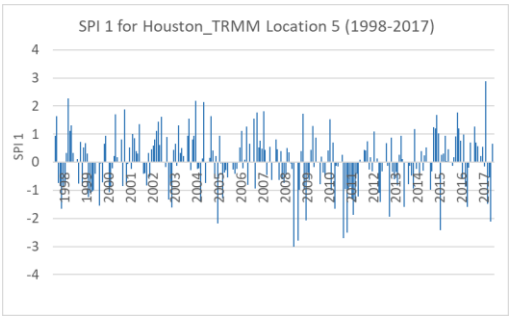
SPI 1 for Houston_TRMM Location 5 (1998-2017)
SPI 1

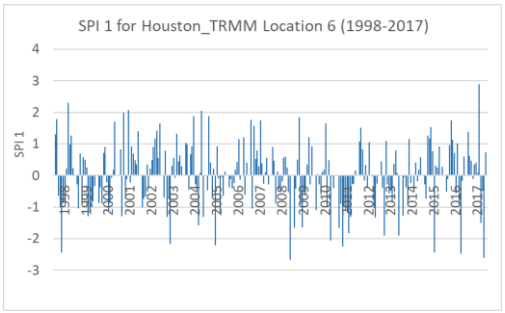
SPI 1 for Houston_TRMM Location 6 (1998-2017)
SPI 1

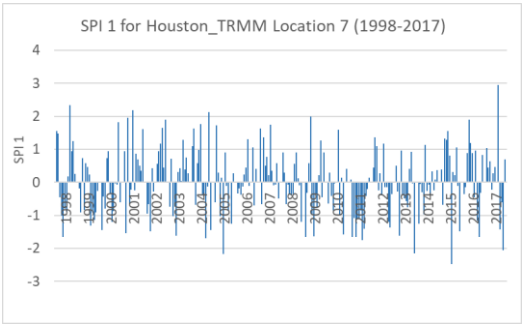
SPI 1 for Houston_TRMM Location 7 (1998-2017)
SPI 1

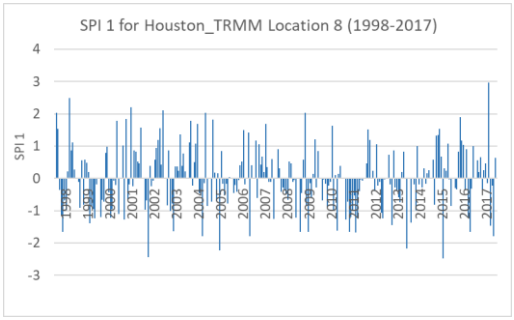
SPI 1 for Houston_TRMM Location 8 (1998-2017)
SPI 1

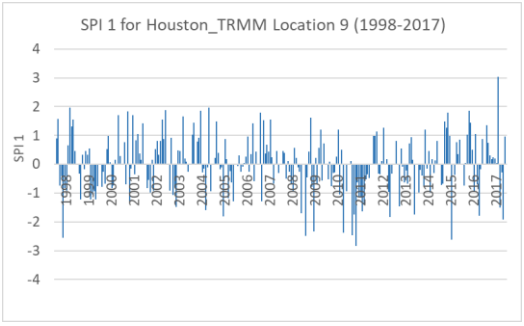
SPI 1 for Houston_TRMM Location 9 (1998-2017)
SPI 1

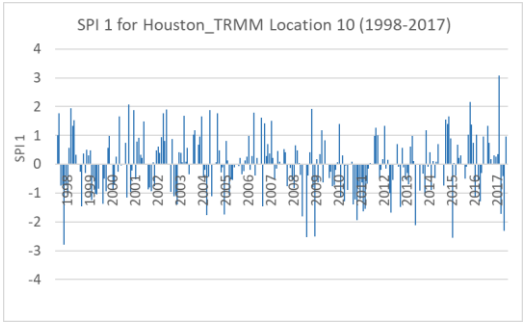
SPI 1 for Houston_TRMM Location 10 (1998-2017)
SPI 1

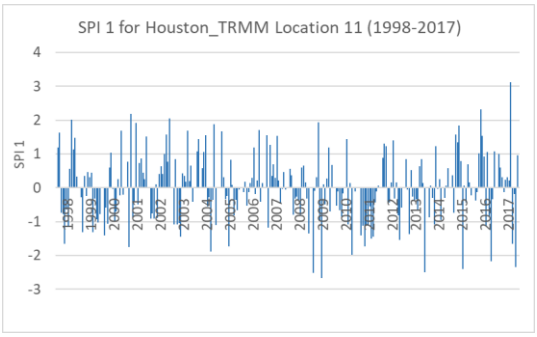

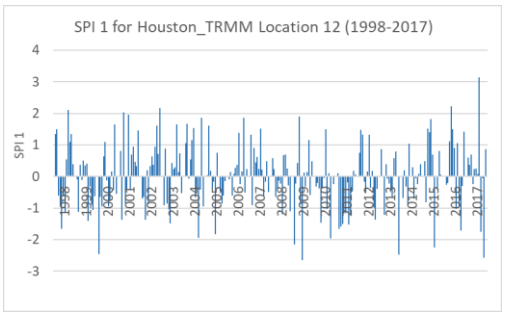

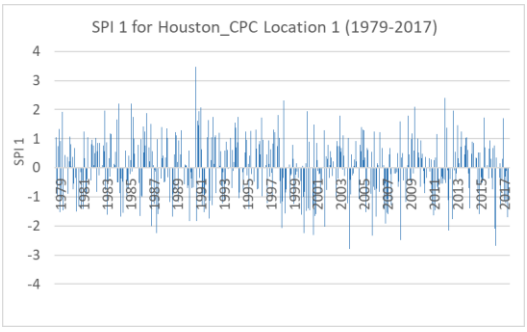

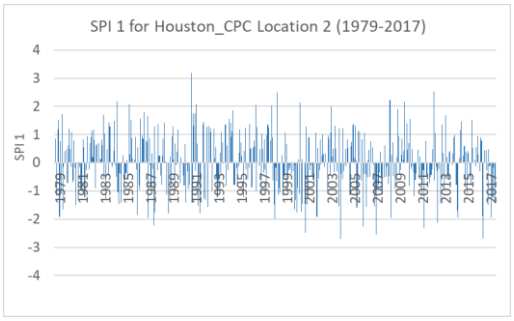

Standardized Precipitation Index Graphs for Mexico City

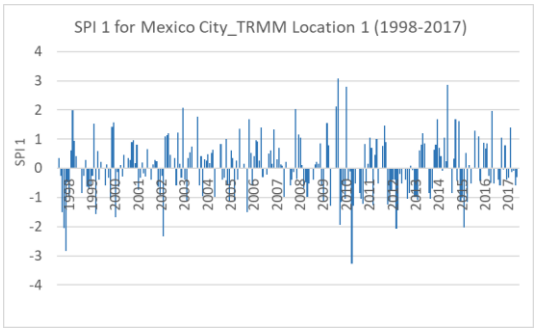

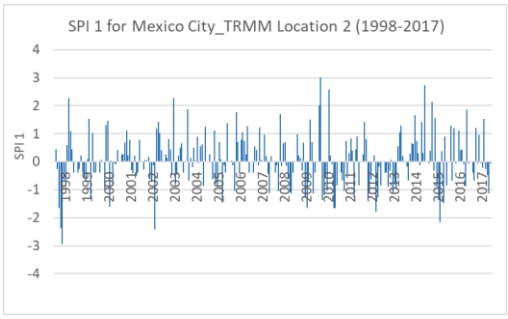

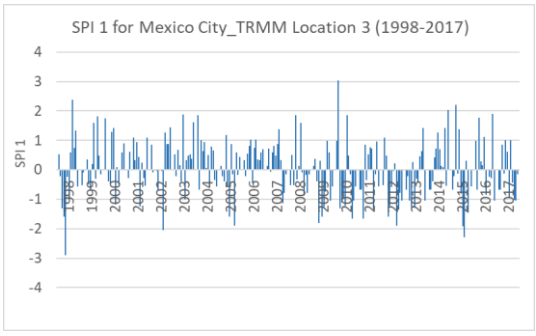

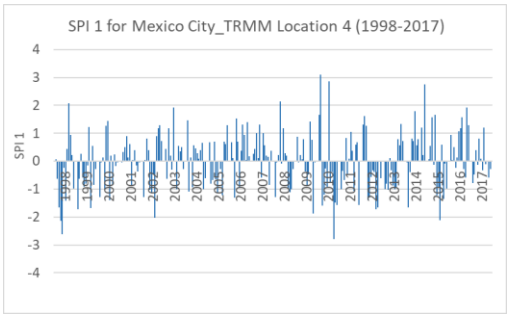

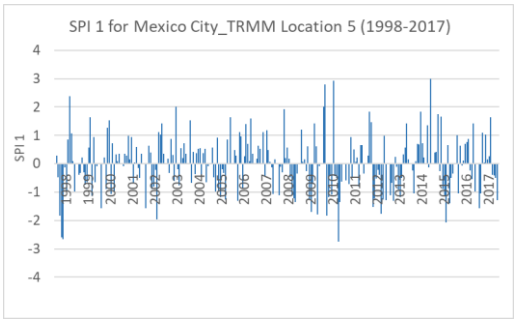

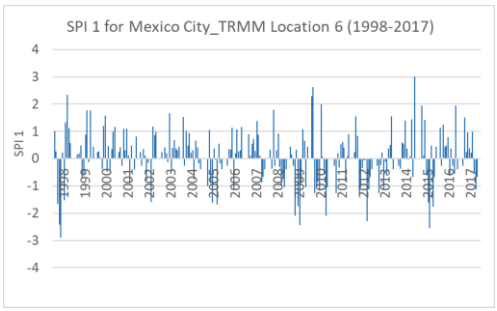

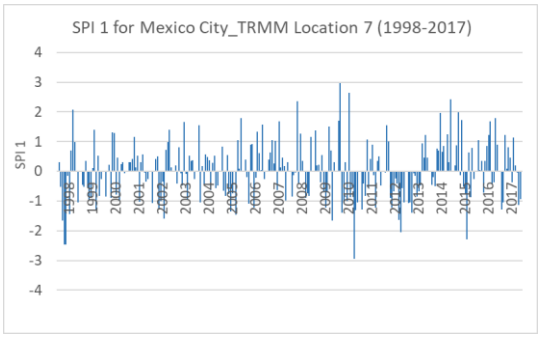

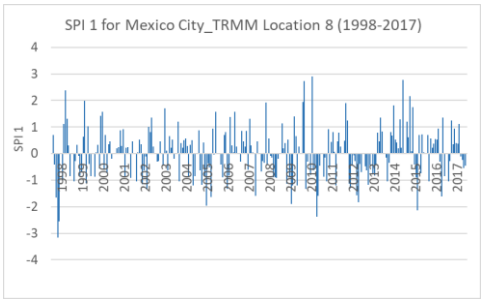

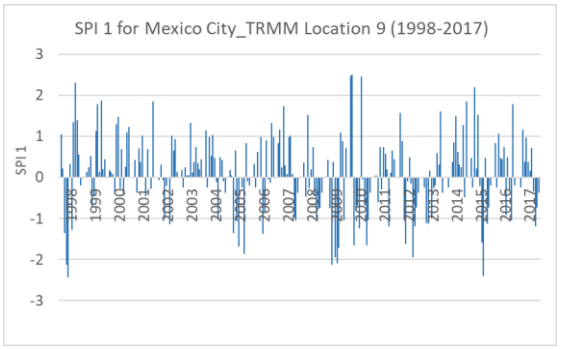

Standardized Precipitation Index Graphs for Jakarta

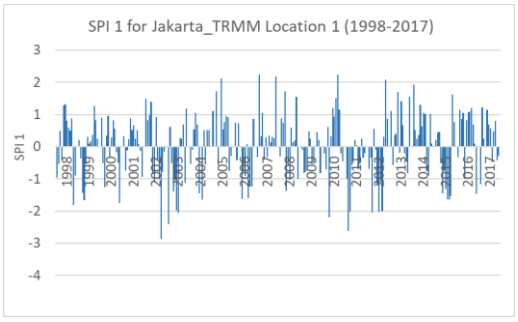

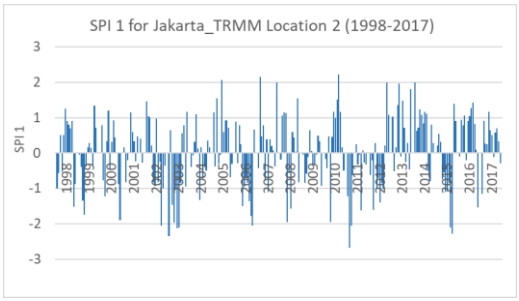

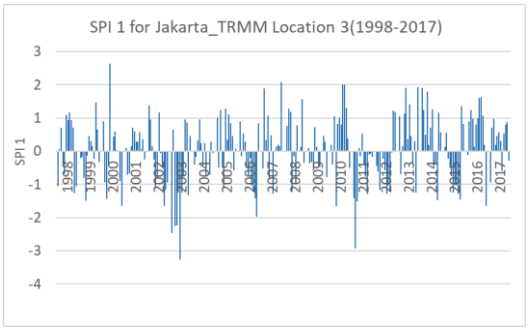

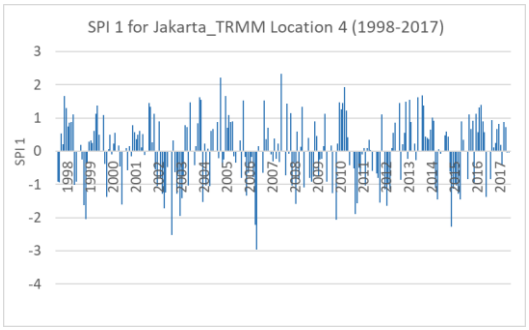

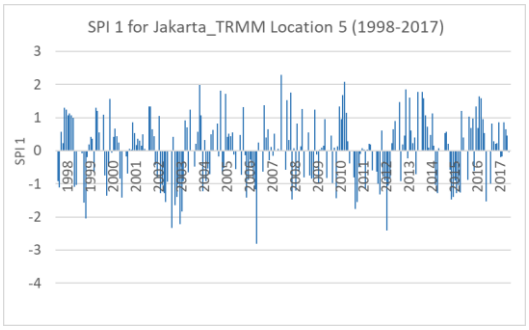

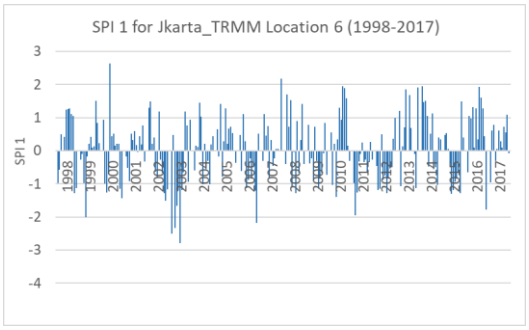

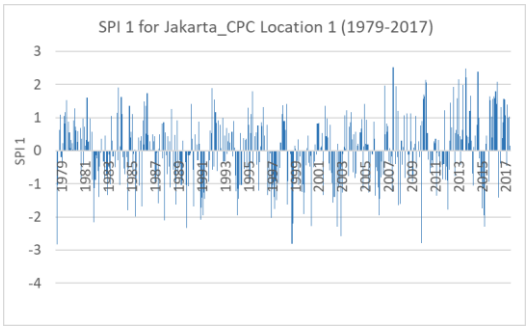

Standardized Precipitation Index Graphs for Dhaka

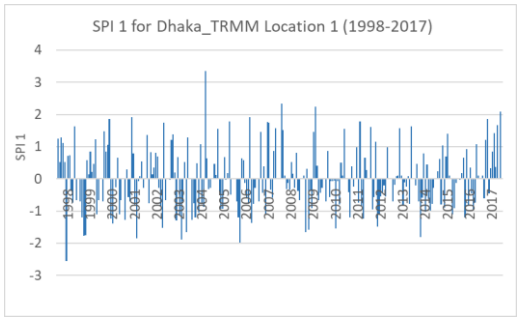

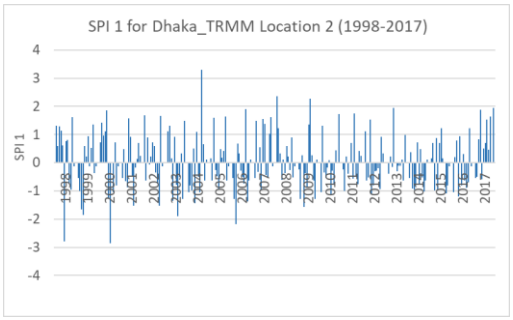

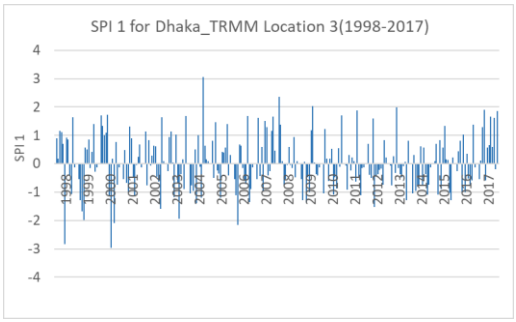
SPI 1 for Dhaka_TRMM Location 3(1998-2017)
SPI 1

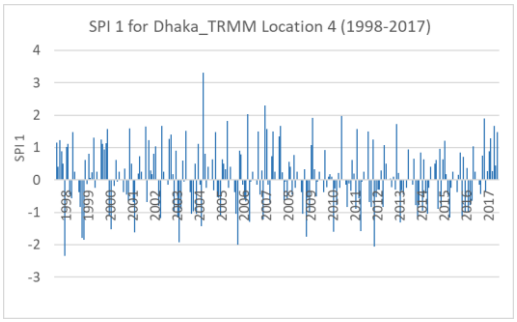
SPI 1 for Dhaka_TRMM Location 4 (1998-2017)
SPI 1

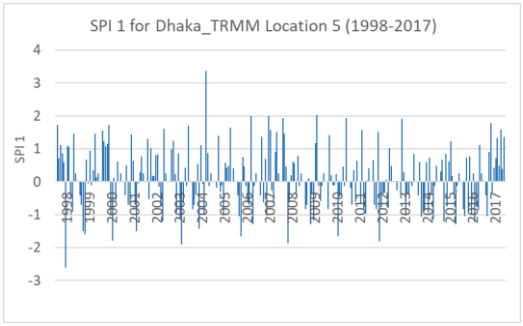
SPI 1 for Dhaka_TRMM Location 5 (1998-2017)
SPI 1

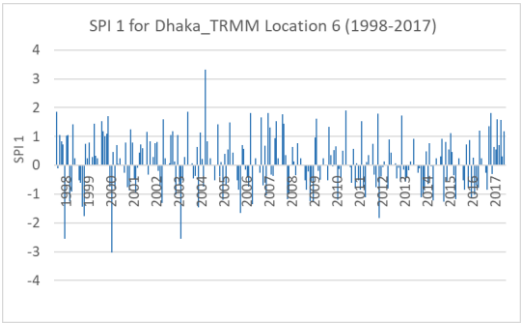
SPI 1 for Dhaka_TRMM Location 6 (1998-2017)
SPI 1

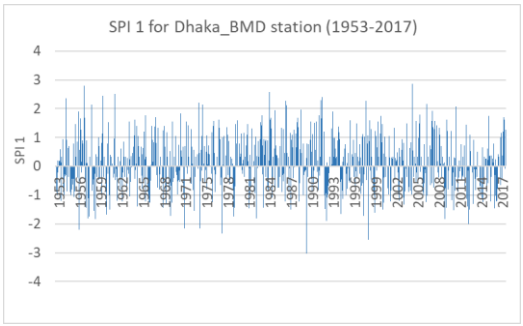
SPI 1 for Dhaka_BMD station (1953-2017)
SPI 1

Appendix VII: Urban Flood Risk Maps

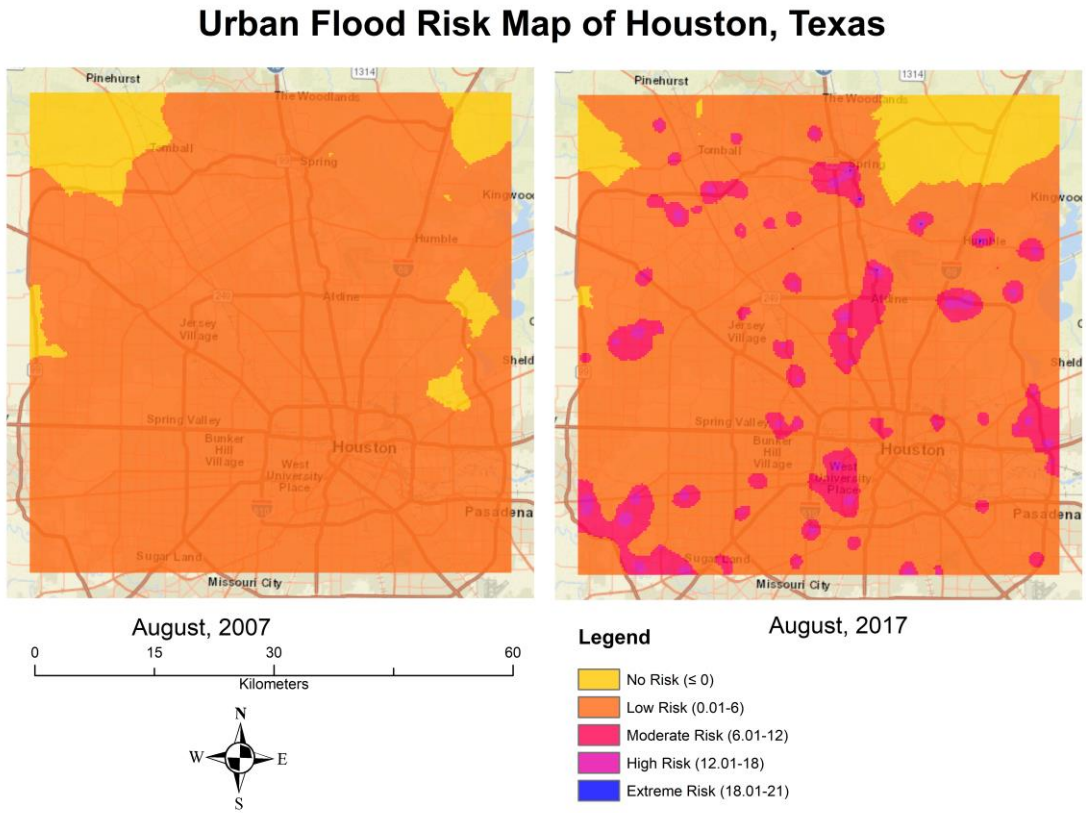

Urban Flood Risk Map of Mexico City, Mexico

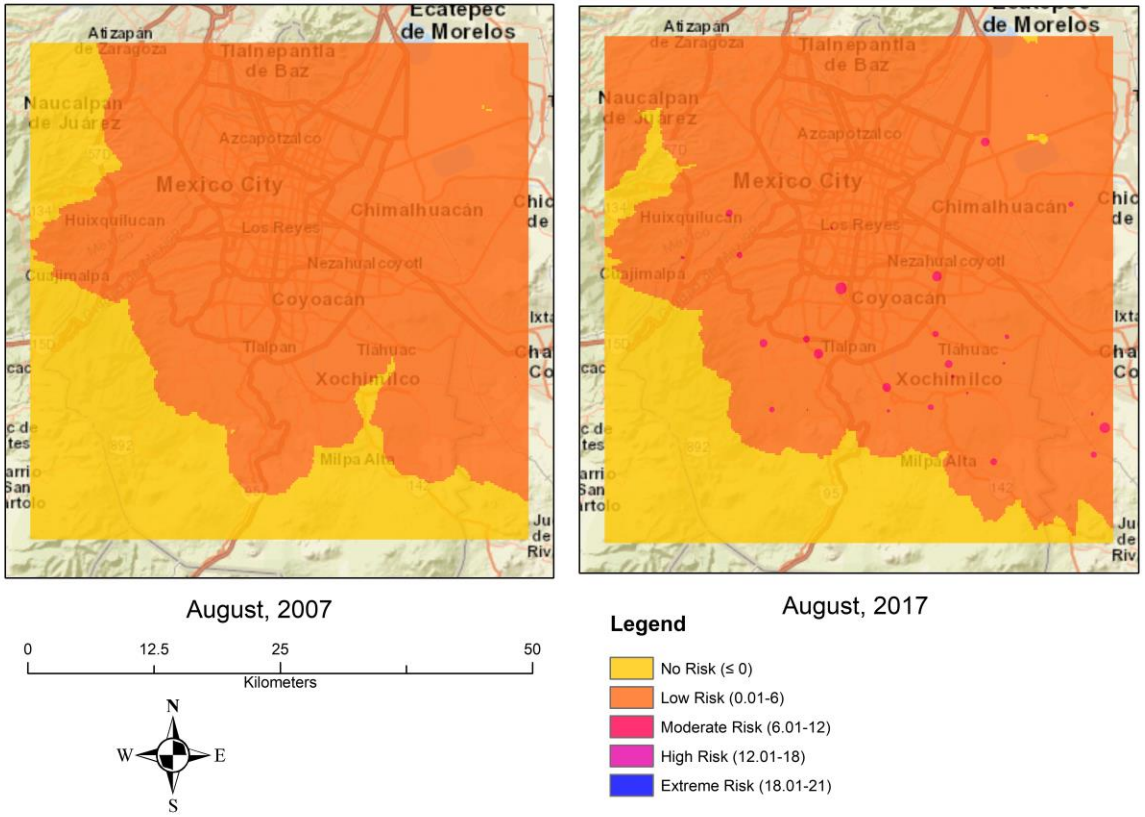

Urban Flood Risk Map of Jakarta, Indonesia

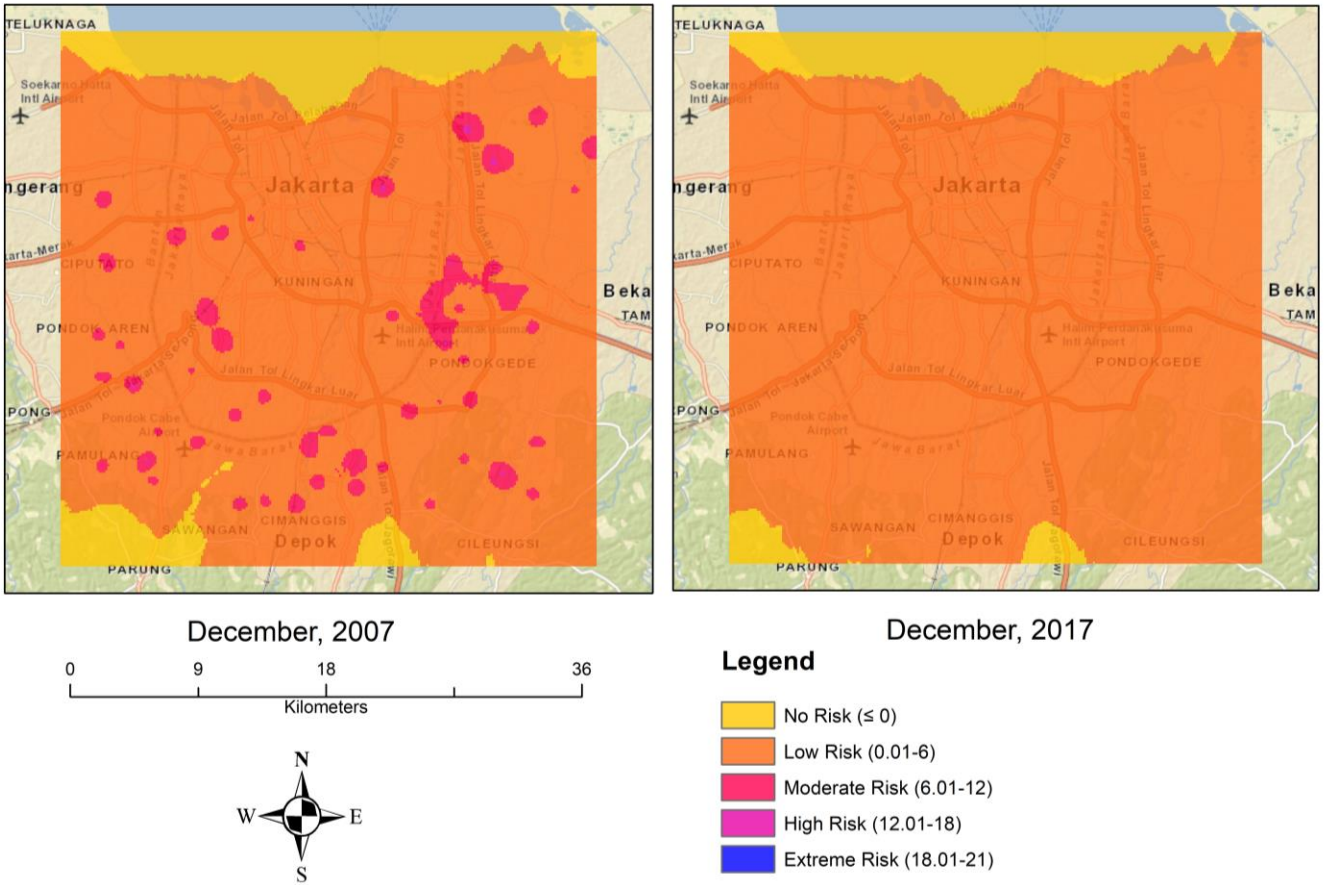

Urban Flood Risk Map of Dhaka, Bangladesh

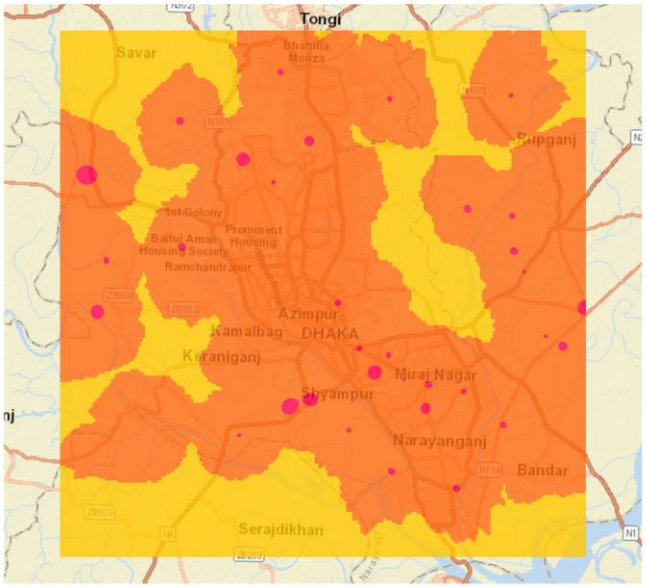

July, 2007

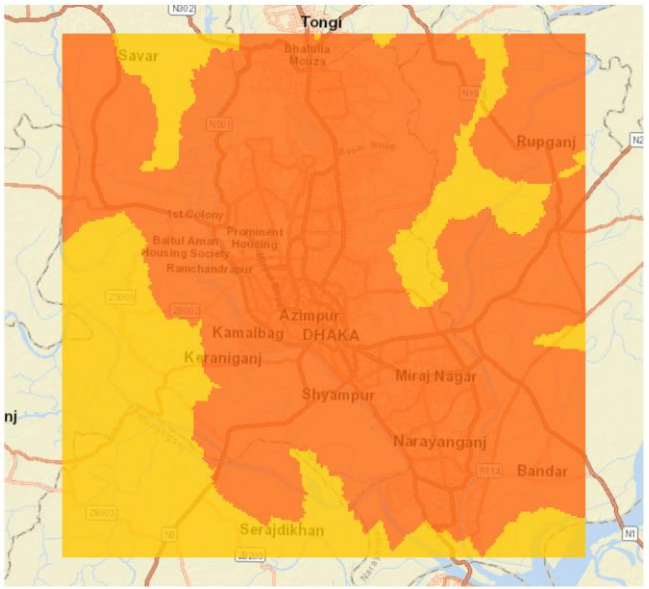

July, 2017

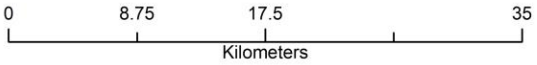

Legend

- No Risk (≤ 0)
- Low Risk (0.01-6)
- Moderate Risk (6.01-12)
- High Risk (12.01-18)
- Extreme Risk (18.01-21)

Bibliography

Adeloye, A. J., & Rustum, R. (2011). Lagos (Nigeria) flooding and influence of urban planning. *Proceedings of the Institution of Civil Engineers-Urban Design and Planning*, *164*(3), 175–187.

Aderogba, K. A. (2012). Qualitative studies of recent floods and sustainable growth and development of cities and towns in Nigeria. *International Journal of Academic Research in Economics and Management Sciences*, *1*(3), 1.

Aderogba, K., Oredipe, M., Oderinde, S., & Afelumo, T. (2012). Challenges of Poor Drainage Systems and Floods in Lagos Metropolis, Nigeria. *International Journal of Social Sciences & Education*, *2*(3).

Adikari, Y., Osti, R., & Noro, T. (2010). Flood-related disaster vulnerability: an impending crisis of megacities in Asia. *Journal of Flood Risk Management*, *3*(3), 185–191.

Akanda, A. S., & Hossain, F. (2012). The climate-water-health nexus in emerging megacities. *Eos, Transactions American Geophysical Union*, *93*(37), 353–354.

Ali, M., Khan, S. J., Aslam, I., & Khan, Z. (2011). Simulation of the impacts of land-use change on surface runoff of Lai Nullah Basin in Islamabad, Pakistan. *Landscape and Urban Planning*, *102*(4), 271–279.

Bass, B., Juan, A., Gori, A., Fang, Z., & Bedient, P. (2016). 2015 Memorial Day Flood Impacts for Changing Watershed Conditions in Houston. *Natural Hazards Review*, *18*(3), 5016007.

Birsan, M.-V., Molnar, P., Burlando, P., & Pfaundler, M. (2005). Streamflow trends in Switzerland. *Journal of Hydrology*, *314*(1–4), 312–329.

Bonaccorso, B., Cancelliere, A., & Rossi, G. (2015). Probabilistic forecasting of drought class transitions in Sicily (Italy) using standardized precipitation index and North Atlantic oscillation index. *Journal of Hydrology*, *526*, 136–150.

Brinkman, J. J., & Hartman, M. (2008). Jakarta flood hazard mapping framework. *World Bank Report(Unpublished). At Http://Www. Hkv. Nl/Documenten/Jakarta_Flood_Hazard_Mapping_Framework_MH. Pdf*.

Brody, S. D., Peacock, W. G., & Gunn, J. (2012). Ecological indicators of flood risk along the Gulf of Mexico. *Ecological Indicators*, *18*, 493–500.

Budiyono, Y., Aerts, J., Brinkman, J., Marfai, M. A., & Ward, P. (2015). Flood risk assessment for delta mega-cities: a case study of Jakarta. *Natural Hazards*, *75*(1), 389–413.

Cohen, J. E. (2003). Human population: the next half century. *Science*, *302*(5648), 1172–1175.

Conlon, K., Monaghan, A., Hayden, M., & Wilhelmi, O. (2016). Potential impacts of future warming and land use changes on intra-urban heat exposure in Houston, Texas. *PloS One*, *11*(2), e0148890.

Damodaram, C., Giacomoni, M. H., Prakash Khedun, C., Holmes, H., Ryan, A., Saour, W., & Zechman, E. M. (2010). Simulation of Combined Best Management Practices and Low Impact Development for Sustainable Stormwater Management 1. *JAWRA Journal of the American Water Resources Association*, *46*(5), 907–918.

Dewan, A. M., & Yamaguchi, Y. (2009). Using remote sensing and GIS to detect and monitor land use and land cover change in Dhaka Metropolitan of Bangladesh during 1960–2005. *Environmental Monitoring and Assessment*, *150*(1–4), 237.

Douglas, E. M., Vogel, R. M., & Kroll, C. N. (2000). Trends in floods and low flows in the United States: impact of spatial correlation. *Journal of Hydrology*, *240*(1–2), 90–105.

Eakin, H., Bojórquez-Tapia, L. A., Janssen, M. A., Georgescu, M., Manuel-Navarrete, D., Vivoni, E. R., … Lerner, A. M. (2017). Opinion: urban resilience efforts must consider social and political forces. *Proceedings of the National Academy of Sciences*, *114*(2), 186–189.

Fang, Z., Safiolea, E., & Bedient, P. B. (2006). Enhanced flood alert and control systems for houston. In *Coastal Hydrology and Processes: Proceedings of the AIH 25th Anniversary Meeting & International Conference Challenges in Coastal Hydrology and Water Quality* (Vol. 199).

Gajbhiye, S., Meshram, C., Mirabbasi, R., & Sharma, S. K. (2016). Trend analysis of rainfall time series for Sindh river basin in India. *Theoretical and Applied Climatology*, *125*(3–4), 593–608.

Goddard Earth Sciences Data and Information Services Center (GES DISC). (n.d.). TRMM_3B42_Daily: TRMM (TMPA) Precipitation L3 1 day 0.25 degree x 0.25 degree V7. Retrieved May 15, 2018, from https://disc.gsfc.nasa.gov/datasets/TRMM_3B42_Daily_V7/summary?keywords=trmm

Gorelick, N., Hancher, M., Dixon, M., Ilyushchenko, S., Thau, D., & Moore, R. (2017). Google Earth Engine: Planetary-scale geospatial analysis for everyone. *Remote Sensing of Environment*, *202*, 18–27. https://doi.org/10.1016/j.rse.2017.06.031

Grineski, S., Collins, T. W., Chakraborty, J., & Montgomery, M. (2015). Hazardous air pollutants and flooding: A comparative interurban study of environmental injustice. *GeoJournal*, *80*(1), 145–158.

Guhathakurta, P., Menon, P., Inkane, P. M., Krishnan, U., & Sable, S. T. (2018). Trends and variability of meteorological drought over the districts of India using

standardized precipitation index. *Journal of Earth System Science*, *127*(1), 2.

Hassan, M. M., & Southworth, J. (2017). Analyzing land cover change and urban growth trajectories of the mega-urban region of Dhaka using remotely sensed data and an ensemble classifier. *Sustainability*, *10*(1), 10.

Hayes, M. J. (2000). Revisiting the SPI: clarifying the process.

Hayes, M. J., Svoboda, M. D., Wilhite, D. A., & Vanyarkho, O. V. (1999). Monitoring the 1996 drought using the standardized precipitation index. *Bulletin of the American Meteorological Society*, *80*(3), 429–438.

Hirsch, R. M., Slack, J. R., & Smith, R. A. (1982). Techniques of trend analysis for monthly water quality data. *Water Resources Research*, *18*(1), 107–121.

Hossain, A. M. M. M., Fien, J., & Horne, R. (2018). Megacity Dhaka:'water security syndrome'and implications for the scholarship of sustainability. *Sustainable Water Resources Management*, *4*(1), 63–78.

Hsiung, B.-C. B., Yang, K.-H., Aila, W., & Ge, L. (2018). Evaluation of the wall deflections of a deep excavation in Central Jakarta using three-dimensional modeling. *Tunnelling and Underground Space Technology*, *72*, 84–96.

Hugh-Jones, M. (1989). Applications of remote sensing to the identification of the habitats of parasites and disease vectors. *Parasitology Today*, *5*(8), 244–251.

IRIN. (2012). Dhaka's shrinking wetlands raise disaster risks. Retrieved from http://www.irinnews.org/feature/2012/06/18

Jacobson, C. R. (2011). Identification and quantification of the hydrological impacts of imperviousness in urban catchments: A review. *Journal of Environmental Management*, *92*(6), 1438–1448.

Jiménez, B., Méndez, J. M., Barrios, J. A., Salgado, G., & Sheinbaum, C. (2004). Characterization and evaluation of potential reuse options for wastewater sludge and combined sewer system sediments in Mexico. *Water Science and Technology*, *49*(10), 171–178.

Kartez, J. D., & Lindell, M. K. (1987). Planning for uncertainty: The case of local disaster planning. *Journal of the American Planning Association*, *53*(4), 487–498.

Kendall, M. G. (1955). Rank correlation methods.

Lall, S. V, Selod, H., & Shalizi, Z. (2006). *Rural-urban migration in developing countries: A survey of theoretical predictions and empirical findings*. The World Bank.

Lamond, J., Bhattacharya, N., & Bloch, R. (2012). The role of solid waste management as a response to urban flood risk in developing countries, a case

study analysis. *WIT Transactions on Ecology and the Environment*, *159*, 193–204.

Landers, J. (2017). Houston Community Converts Golf Course into Detention System, Natural Areas. *Civil Engineering*, *87*(11).

Larasati, D. A., & Hariyanto, B. (2018). The impact of land use changes in the Banjarsari village, Cerme district of Gresik Regency, East Java Province. In *Journal of Physics: Conference Series* (Vol. 953, p. 12178). IOP Publishing.

Leopold, L. B., Wolman, M. G., & Miller, J. P. (2012). *Fluvial processes in geomorphology*. Courier Corporation.

Loch, R. J. (2000). Effects of vegetation cover on runoff and erosion under simulated rain and overland flow on a rehabilitated site on the Meandu Mine, Tarong, Queensland. *Soil Research*, *38*(2), 299–312.

Lynn, K. A. (2017). Who defines' whole': an urban political ecology of flood control and community relocation in Houston, Texas. *Journal of Political Ecology*, *24*(1), 951–967.

Mann, H. B. (1945). Nonparametric tests against trend. *Econometrica: Journal of the Econometric Society*, 245–259.

Mark, O., Apirumanekul, C., Kamal, M. M., & Praydal, G. (2001). Modelling of urban flooding in Dhaka City. In *Urban Drainage Modeling* (pp. 333–343).

Mark, O., Wennberg, C., Van Kalken, T., Rabbi, F., & Albinsson, B. (1998). Risk analyses for sewer systems based on numerical modelling and GIS. *Safety Science*, *30*(1–2), 99–106.

McKee, T. B. (1995). Drought monitoring with multiple time scales. In *Proceedings of 9th Conference on Applied Climatology, Boston, 1995*.

McKee, T. B., Doesken, N. J., & Kleist, J. (1993). The relationship of drought frequency and duration to time scales. In *Proceedings of the 8th Conference on Applied Climatology* (Vol. 17, pp. 179–183). American Meteorological Society Boston, MA.

Muñoz, L. A., Olivera, F., Giglio, M., & Berke, P. (2018). The impact of urbanization on the streamflows and the 100-year floodplain extent of the Sims Bayou in Houston, Texas. *International Journal of River Basin Management*, *16*(1), 61–69.

NOAA/OAR/ESRL PSD, Boulder, Colorado, U. (n.d.). CPC Global Unified Gauge-Based Analysis of Daily Precipitation. Retrieved from https://www.esrl.noaa.gov/psd/data/gridded/data.cpc.globalprecip.html

Ochoa, C. A., Quintanar, A. I., Raga, G. B., & Baumgardner, D. (2015). Changes in intense precipitation events in Mexico City. *Journal of Hydrometeorology*, *16*(4), 1804–1820.

Odunuga, S. S. (2008). Urban Land Use Change and the Flooding Patterns in Ashimowu Watershed, Lagos, Nigeria.

Padawangi, R., & Douglass, M. (2015). Water, water everywhere: toward participatory solutions to chronic urban flooding in Jakarta. *Pacific Affairs*, *88*(3), 517–550.

Pal, S., & Ziaul, S. (2017). Detection of land use and land cover change and land surface temperature in English Bazar urban centre. *The Egyptian Journal of Remote Sensing and Space Science*, *20*(1), 125–145.

Pangaribowo, R. L. (2018). Dynamics of land-use change in urban area in West Jakarta. In *IOP Conference Series: Earth and Environmental Science* (Vol. 106, p. 12040). IOP Publishing.

Platt, H. L. (2010). Exploding cities: housing the masses in Paris, Chicago, and Mexico City, 1850—2000. *Journal of Urban History*, *36*(5), 575–593.

Quintana-Belmares, R. O., Krais, A. M., Esfahani, B. K., Rosas-Pérez, I., Mucs, D., López-Marure, R., … Alfaro-Moreno, E. (2018). Phthalate esters on urban airborne particles: Levels in PM 10 and PM 2.5 from Mexico City and theoretical assessment of lung exposure. *Environmental Research*, *161*, 439–445.

Rahman, M. Z., Kamal, A. S. M. M., & Siddiqua, S. (2018). Near-surface shear wave velocity estimation and V s 30 mapping for Dhaka City, Bangladesh. *Natural Hazards*, *92*(3), 1687–1715.

Romero Lankao, P. (2010). Water in Mexico City: what will climate change bring to its history of water-related hazards and vulnerabilities? *Environment and Urbanization*, *22*(1), 157–178.

Seiler, R. A., Hayes, M., & Bressan, L. (2002). Using the standardized precipitation index for flood risk monitoring. *International Journal of Climatology*, *22*(11), 1365–1376.

Sen, P. K. (1968). Estimates of the regression coefficient based on Kendall's tau. *Journal of the American Statistical Association*, *63*(324), 1379–1389.

Siemens, J., Huschek, G., Siebe, C., & Kaupenjohann, M. (2008). Concentrations and mobility of human pharmaceuticals in the world's largest wastewater irrigation system, Mexico City–Mezquital Valley. *Water Research*, *42*(8–9), 2124–2134.

Singh, P., Kumar, V., Thomas, T., & Arora, M. (2008). Changes in rainfall and relative humidity in river basins in northwest and central India. *Hydrological Processes*, *22*(16), 2982–2992.

Tellman, B., Bausch, J., Eakin, H., Anderies, J., Mazari-Hiriart, M., Manuel-Navarrete, D., & Redman, C. (2018). Adaptive pathways and coupled infrastructure: seven centuries of adaptation to water risk and the production of vulnerability in Mexico City. *Ecology and Society*, *23*(1).

The World Bank. (2011). *Indonesia -Jakarta Urgent Flood Mitigation Project (Jakarta Emergency Dredging Initiative)*. Retrieved from http://projects.worldbank.org/P111034/jakarta-urgent-flood-mitigation-project?lang=en

The World Bank. (2017). Toward Great Dhaka. Retrieved from http://www.worldbank.org/en/news/speech/2017/07/19/toward-great-dhaka

Torres-Vera, M. A., Prol-Ledesma, R. M., & García-López, D. (2009). Three decades of land use variations in Mexico City. *International Journal of Remote SensingInternational Journal of Remote Sensing*, *30*(1), 117–138.

USGS. (2017). EarthExplorer. Retrieved from https://earthexplorer.usgs.gov/

Verburg, P. H., & Bouma, J. (1999). Land use change under conditions of high population pressure: the case of Java. *Global Environmental Change*, *9*(4), 303–312.

Walker, G., Whittle, R., Medd, W., & Walker, M. (2011). Assembling the flood: producing spaces of bad water in the city of Hull. *Environment and Planning A*, *43*(10), 2304–2320.

Wheater, H., & Evans, E. (2009). Land use, water management and future flood risk. *Land Use Policy*, *26*, S251–S264.

Xian, S., Lin, N., & Hatzikyriakou, A. (2015). Storm surge damage to residential areas: a quantitative analysis for Hurricane Sandy in comparison with FEMA flood map. *Natural Hazards*, *79*(3), 1867–1888.

Yasmin, S., & Rahman, M. I. (2017). A Review of Solid Waste Management Practice in Dhaka City, Bangladesh. *International Journal of Environmental Protection and Policy*, *5*(2), 19.

Yu, Y.-S., Zou, S., & Whittemore, D. (1993). Non-parametric trend analysis of water quality data of rivers in Kansas. *Journal of Hydrology*, *150*(1), 61–80.

Zambrano, L., Pacheco-Muñoz, R., & Fernández, T. (2018). Influence of solid waste and topography on urban floods: The case of Mexico City. *Ambio*, 1–10.

Zhang, G., Qian, Y., Wang, Z., & Zhao, B. (2014). Analysis of rainfall infiltration law in unsaturated soil slope. *The Scientific World Journal*, *2014*.

Zhang, Q., Xu, C.-Y., & Zhang, Z. (2009). Observed changes of drought/wetness episodes in the Pearl River basin, China, using the standardized precipitation index and aridity index. *Theoretical and Applied Climatology*, *98*(1–2), 89–99.